Real-Time Quantitative Reverse Transcription Polymerase Chain Reaction

Real-time polymerase chain reaction amplification was performed with the rabbit cDNA with the use of the ABI PRISM 7000 Sequence Detection System (Applied Biosystems, Foster City, Calif) as described previously.[22] The respective polymerase chain reaction primers and TaqMan probes were designed from GenBank databases with a software program (Applied Biosystems; Table II in the online-only Data Supplement).

Fluorescence-Activated Cell Sorting

Peripheral blood was obtained at day 10 after stent implantation (n=7 each). Flow cytometry for $CD14^+$ cells was performed with the use of R-phycoerythrin–conjugated anti-CD14 (Dako). Data were analyzed by a flow cytometer and software (Becton, Dickinson and Co, Franklin Lakes, NJ).

Blood Cholesterol Measurements

Plasma total cholesterol levels were determined with commercially available kits (Wako Pure Chemical Industries, Ltd, Osaka, Japan).

Human Coronary Artery Smooth Muscle Cell Culture

This section is available in the online-only Data Supplement.

Potential Systemic Adverse Effects or Toxicity

To examine systemic adverse effects, biochemical markers were measured before and after implantation of the NF-κB decoy–eluting stent in rabbits (n=7). Five 5-year-old male cynomolgus monkeys weighing 4.2 to 5.0 kg were purchased and fed a normal diet (n=5). Biochemical markers were measured before and after intravenous injection of NF-κB decoy at 1 mg.

Statistical Analysis

Data are expressed as mean±SD. Statistical analysis of differences between the 2 groups was performed by unpaired *t* test. Statistical analysis of differences among the 3 groups was performed with the use of ANOVA and Bonferroni multiple comparison tests. A level of $P<0.05$ was considered statistically significant.

The authors had full access to the data and take responsibility for the integrity of the data. All authors have read and agree to the manuscript as written.

Results

Eluting Stent and In Vitro Release Kinetics

Scanning electron microscopy analysis revealed that the polymer coating formed a uniform film over the outer surface of the stent (Figure 1A). After balloon expansion, stretching of the polymer with no fragmentation was observed (Figure 1A). In vitro release kinetics showed an early burst release of NF-κB decoy as designed (Figure 1B).

Early Activation of NF-κB After Stenting and Effects of NF-κB Decoy–Eluting Stents

Time course and localization of NF-κB activation were examined by immunohistochemical studies with the antibody against α-p65. This antibody recognizes the I-κB binding region on the p65 component of NF-κB.[11] In the unstented artery, no positive cells for α-p65 were noted in the media and adventitia, whereas there were some positive cells in the endothelial layer (Figure 2A). On day 3, activation of NF-κB was noted in the smooth muscle cells in the media. On day 10, activation of NF-κB decreased markedly in the media, but it was noted in neointimal cells of the luminal side. On day 28,

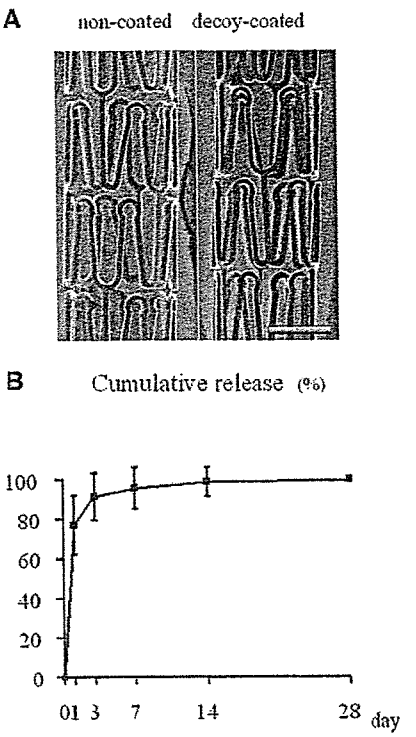

Figure 1. A, Scanning electron microscopic images of balloon-expanded uncoated stent (left) and NF-κB decoy–coated stent (right). Scale bar=1 mm. B, In vitro time course of cumulative NF-κB decoy release from the eluting stents (n=8). The percentage of incremental quantities of the decoy released from the stent was plotted against time.

NF-κB activation was rarely noted in the media and neointima, but it was noted in cells around the stent strut.

The effects of NF-κB decoy–eluting stent on NF-κB activation were examined on day 3 (Figure 2B and 2C). As expected, compared with the uncoated stent site, the number of α-p65–positive cells in the media was less ($P<0.01$) in the NF-κB decoy–eluting stent site.

To confirm immunohistochemical data, an electrophoretic mobility shift assay was performed (Figure 3). No DNA binding activity of NF-κB was noted in samples from unstented arteries. In contrast, the binding activity increased strikingly in samples from the uncoated stent site, which peaked on day 1 and gradually decreased on days 3 and 7. This NF-κB binding activity was attenuated in samples from the NF-κB–eluting stent site. Competition for increased binding of NF-κB was observed by an excess amount of NF-κB. A diminution of main band with supershifted band was observed in samples from uncoated stent sites treated with the p65 antibody but not with the p50 antibody.

Inhibitory Effects of NF-κB Decoy–Eluting Stent on Neointimal Formation

The in-stent neointima was formed equally in the uncoated stent and polyurethane-coated stent sites. Quantitative analysis demonstrated a significant reduction ($P<0.01$) of neointimal formation (neointimal area and thickness) and percent stenosis in the NF-κB decoy–eluting stent site compared with the other 2 sites (Figure 4). In contrast, there were no

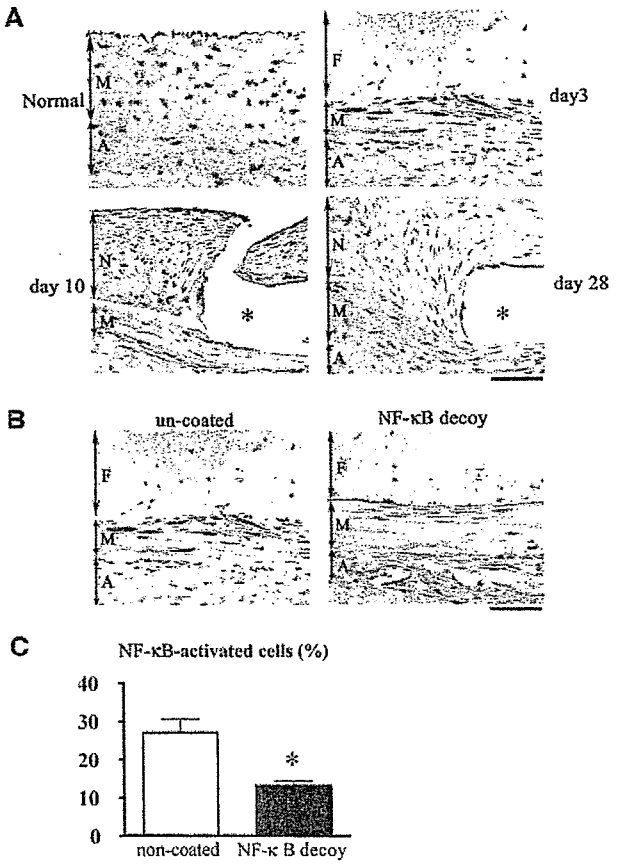

Figure 2. Immunohistochemical detection of activated NF-κB after stenting and inhibitory effects of NF-κB decoy–eluting stents on NF-κB activation. A, Immunohistochemistry of arterial cross sections stained with α-p65. *Stent strut. F indicates fibrin layer; N, neointima; M, media; and A, adventitia. Bar=50 μm. B, Artery sections from the uncoated stent site and NF-κB–eluting stent site stained immunohistochemically with the antibody against α-p65. *Stent strut. Bar=50 μm. C, Comparison of NF-κB activity between uncoated stent and NF-κB–eluting stent sites (n=6 each). Percentage of NF-κB–activated (α-p65–positive) cells is shown. *$P<0.01$ vs uncoated stents by unpaired t test.

significant differences in internal elastic lamina area, external elastic lamina area, and medial area among the 3 groups.

A semiquantitative histological scoring system demonstrated that there was no significant difference in the injury score and inflammation score among the 3 groups (Table I in the online-only Data Supplement). Endothelial cell linings, monitored by CD31 immunoreactivity, were observed equally in the 3 groups (Table I in the online-only Data Supplement). There was no significant treatment effect on serum cholesterol levels and body weight among the groups (data not shown).

Inhibitory Effects of NF-κB Decoy–Eluting Stents on Local and Systemic Inflammatory Changes

As we previously reported,[9] infiltration of RAM-11–positive macrophages around stent strut was observed at 10 days after stent implantation (Figure 5A). NF-κB decoy–eluting stents reduced such inflammatory changes (Figure 5B).

CD14 expression on circulating monocytes was examined by flow cytometry for $CD14^+$ cells as a systemic inflammation marker. Maximum fluorescence intensity of CD14 on circulating monocytes increased ($P<0.01$) 10 days after uncoated stent implantation compared with unstented controls. No increase in CD14 expression on monocytes was observed in animals implanted with NF-κB decoy–eluting stent (Figure 5C).

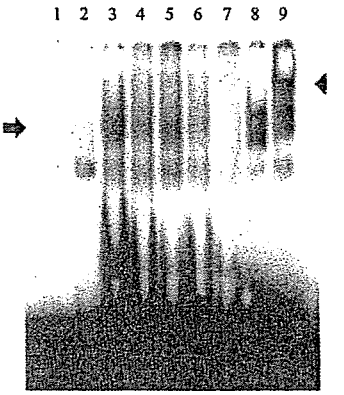

Figure 3. Assessment of activated NF-κB/DNA binding activity by electrophoretic mobility shift assay. NF-κB/DNA binding activity is determined with the use of nuclear extracts isolated from unstented and stented arteries. Lane 1, negative control (^{32}P-labeled NF-κB oligodeoxynucleotide without nuclear extract); lane 2, unstented artery; lane 3, 1-day artery after uncoated stent implantation; lane 4, 3-day artery after uncoated stent implantation; lane 5, 7-day artery after uncoated stent implantation; lane 6, 1-day artery after NF-κB decoy–eluting stent implantation; lane 7, 1-day artery after uncoated stent implantation incubated with extra amount of cold NF-κB oligodeoxynucleotide; lane 8, 1-day artery after uncoated stent implantation incubated with p50 antibody; lane 9, 1-day artery after uncoated stent implantation incubated with p65 antibody; arrowhead indicates supershift.

Inhibitory Effects of NF-κB Decoy–Eluting Stents on Expression of Proinflammatory Factors

NF-κB decoy–eluting stents reduced the increased ($P<0.01$) gene expression of MCP-1, interleukin-6, tumor necrosis factor-α, and tissue factor (Figure 6A). NF-κB decoy–eluting stents did not affect increased gene expression of interleukin-1β and vascular cell adhesion molecule-1. Immunohistochemical staining performed 10 days after stenting revealed increased immunoreactive MCP-1 in cells in the neointima and smooth muscle cells in the media, which was attenuated ($P<0.01$) in the NF-κB decoy–eluting stent group (Figure 6B).

Blockade of NF-κB Inhibits Proliferation of Human Coronary Artery Smooth Muscle Cells

The serum-induced proliferation of human coronary artery smooth muscle cells was nearly prevented ($P<0.01$) by the adenovirus-mediated gene transfer of dominant-active I-κB or by transfection of NF-κB decoy (Figure in the online-only Data Supplement).

No Adverse Systemic Effects of NF-κB Decoy

Biochemical markers were measured as described in the online-only Data Supplement. These data show that no systemic adverse effects of NF-κB decoy were noted in rabbits or monkeys.

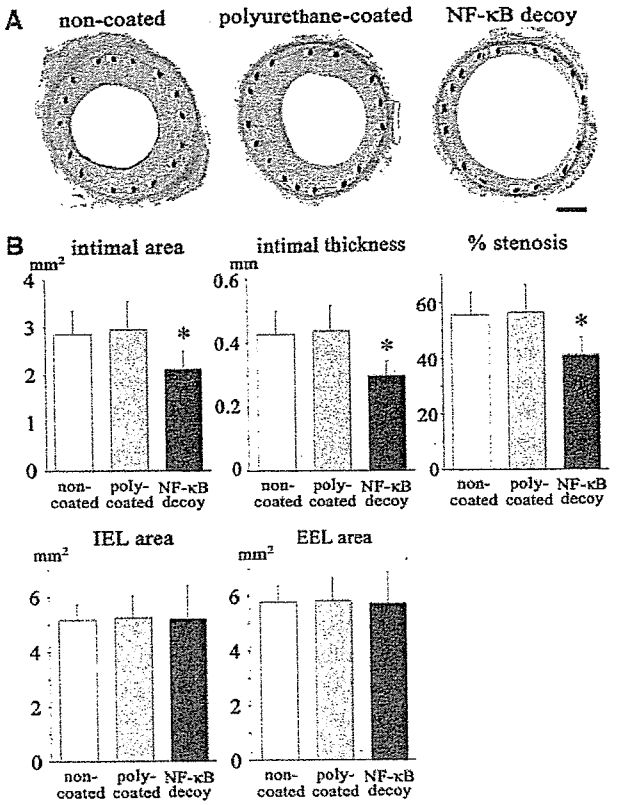

Figure 4. Inhibitory effect of NF-κB decoy–eluting stents on in-stent neointima formation. A, Iliac artery sections from the uncoated, polyurethane (poly)-coated, and NF-κB decoy–eluting stents 28 days after stenting stained with elastica van Gieson in rabbits. Bar=500 μm. B, Effect of the NF-κB decoy–eluting stents on intimal area, intimal thickness, internal elastic lamina (IEL) area, external elastic lamina (EEL) area, and percent stenosis 28 days after stenting in rabbits (n=8 each). *$P<0.01$ vs uncoated stents by ANOVA and Bonferroni multiple comparison tests.

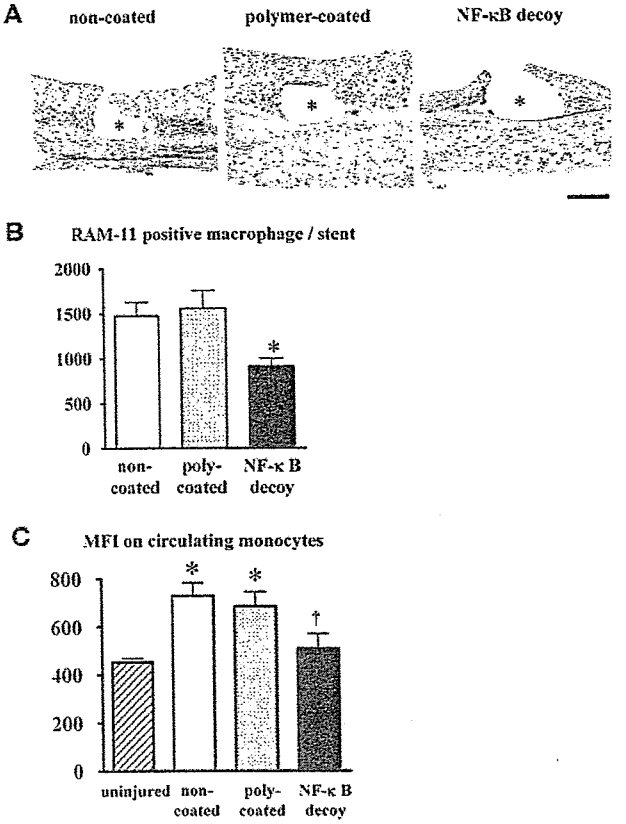

Figure 5. Effects of NF-κB decoy–eluting stents on local and systemic inflammation. A, Effect of NF-κB decoy–eluting stent on local inflammation (RAM-11–positive monocyte/macrophage) 10 days after stenting. *Stent strut. Bar=100 μm. B, Summary of quantitative analysis (n=7 each). Poly indicates polymer. *$P<0.01$ vs uncoated stents. C, Effects of NF-κB decoy–eluting stent on maximum fluorescence intensity (MFI) of CD14 on circulating monocytes 7 days after stenting (n=7 each). *$P<0.01$ vs unstented rabbits; †$P<0.01$ vs rabbits implanted with uncoated stents by ANOVA and Bonferroni multiple comparison tests.

Discussion

The present study reports, for the first time, the formulation of a stent-based delivery system of the NF-κB decoy oligodeoxynucleotide. A water-soluble polymer (polyurethane) was used to create a rapid-release type because NF-κB was found to be activated only at early stages but not at later stages after stenting. The present study clearly showed early activation of NF-κB after uncoated bare stenting and its inhibition by stent-based local delivery of NF-κB decoy in 2 approaches (immunostaining of a specific marker of NF-κB activation and DNA-finding assay). The inhibition of NF-κB activation was associated with reduced inflammatory changes such as reduced CD14 expression on circulating leukocytes as well as monocyte recruitment into stent sites. Although multiple factors are involved in the mechanism of decoy transfection, the mechanical force during stent expansion by the balloon dilatation procedure is likely to be a major contributing factor. The decoy might be transfected into medial and neointimal smooth muscle cells, which in turn reduced expression of various NF-κB–dependent inflammation-promoting factors. This polymeric technology-driven delivery system could be used for delivery of any other potential candidates of decoy oligodeoxynucleotides.

It has been reported that prolonged inflammatory changes were detected in arteries exposed to polymeric stent-coating materials in experimental animals[18,23] and humans.[3–5] However, no such adverse reaction was noted in this study. In addition, there was no evidence of an impaired healing process and endothelial regeneration at sites of stents coated with polyurethane alone and polyurethane plus decoy. These data suggest that the polymers used in this study may not cause an adverse reaction during a 4-week observation period.

The most important finding of the present study was inhibition of neointimal formation by stent-based delivery of NF-κB decoy. The beneficial effects of NF-κB decoy–eluting stents were associated with reduced gene expression of NF-κB–dependent genes (eg, MCP-1, interleukin-1β, interleukin-6) and with no change in NF-κB–independent genes (platelet-derived growth factor) (Figure 6). Immunoreactive MCP-1 expression was also reduced at sites of NF-κB decoy–eluting stent. These data indicate a specific function of the NF-κB decoy–eluting stent on local NF-κB activation. It is known that injury-induced inflammatory and proliferative

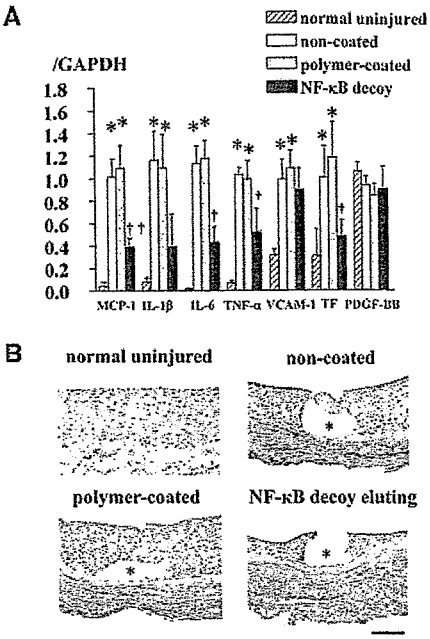

Figure 6. Effects of NF-κB decoy–eluting stents on gene expression of proinflammatory factors and immunohistochemical expression of MCP-1. A, Effect of NF-κB decoy–eluting stents on mRNA levels of various proinflammatory factors and tissue factor (TF) 10 days after stenting (n=7 to 8 each). *$P<0.01$ vs uninjured normal artery; †$P<0.05$, ††$P<0.01$ vs the control group by ANOVA and Bonferroni multiple comparison tests. B, Iliac artery sections from the uninjured normal rabbits and those from the uncoated, polyurethane-coated, and NF-κB decoy–eluting stents implanted in rabbits 10 days after stenting stained immunohistochemically with MCP-1. IL indicates interleukin; TNF, tumor necrosis factor; VCAM, vascular cell adhesion molecule; and PDGF, platelet-derived growth factor. *Stent strut. Bar=100 μm.

changes are critical in restenotic changes after vascular injury.[8,24,25] We and others have reported that (1) increased monocyte-mediated inflammation correlates positively with in-stent neointimal formation[7,26] and (2) blockade of MCP-1 reduces neointimal formation after vascular injury.[9,27,28] Because the NF-κB–eluting stent reduced inflammation and MCP-1 expression in this study, the beneficial effects of NF-κB decoy–eluting stents can be attributable at least in part to inhibition of MCP-1–related inflammation resulting from reduced NF-κB activation. Otherwise, emerging evidence suggests that NF-κB regulates proliferation of vascular smooth muscle cells.[29,30] In this regard, we found that blockade of NF-κB activation by transfection of NF-κB decoy or dominant-active I-κB suppressed proliferation of human coronary artery smooth muscle cells in vitro. Therefore, it is also likely that NF-κB decoy–eluting stents might inhibit proliferation of vascular smooth muscle cells induced by NF-κB activation.

There are several caveats in our present findings in regard to potential clinical applicability. First, application of the present findings to treatment of restenosis in humans could be limited because the ideal animal model for drug-eluting stent evaluation is uncertain according to the recommendation from the consensus group.[31] They stated that the coronary arteries in pigs and iliac-femoral arteries of rabbits are suitable in that their size, access, and injury response are similar to those of human vessels and therefore they allow examination of devices that might be used in clinical evaluation. Thus, the rabbit peripheral artery model is considered an acceptable model of choice. Second, the observed efficacy and safety of NF-κB decoy and polymer at 28 days may be too short. Third, potential adverse effects or toxicity of NF-κB decoy may be important. In histopathological analysis, no adverse reactions such as incomplete healing or impaired endothelial regeneration were noted. Measurements of serum blood markers (glucose, aspartate aminotransferase, alanine aminotransferase, creatine kinase, γ-GTP, and C-reactive protein in Tables III and IV in the online-only Data Supplement) showed no systemic adverse effects. Because the dose of NF-κB decoy (500 to 600 μg per body) coated on the stent was very low from a toxicological point of view, our decoy-coated stent may not cause any toxicity in vivo. It has been reported that repeated bolus administration of high doses (eg, 10 mg/kg every other day for 28 days in monkeys, 20 mg/kg every other day for 28 days in mice) causes kidney damage.[32] In addition, we recently completed a clinical trial to test the feasibility and safety of NF-κB decoy in which NF-κB decoy at doses of 1000, 2000, or 4000 μg per body was transfected into the stented coronary artery sites via a channel balloon catheter immediately after successful percutaneous coronary intervention in 16 patients with flow-limiting coronary stenosis. The initial 2 cases have been reported,[33] and they showed no evidence of restenosis or systemic adverse effects during the 6-month observation period. Overall, these data support the notion that this NF-κB decoy–eluting stent system can be applied to the clinical setting.

In conclusion, the present study supports the experimental evidence that stent-based local delivery of NF-κB decoy reduces in-stent neointimal formation by inhibiting NF-κB–dependent gene expression and inflammation and perhaps by inhibiting proliferation of vascular smooth muscle cells. Inhibition of stent-associated inflammation by the NF-κB decoy–eluting stent may be a promising next-generation approach for the prevention of restenosis. Further preclinical studies and clinical trials are needed to prove this hypothesis.

Sources of Funding

This study was supported by grants-in-aid for scientific research (14657172, 14207036) from the Ministry of Education, Science, and Culture, Tokyo, Japan; by health science research grants (Research on Translational Research) from the Ministry of Health, Labor, and Welfare, Tokyo, Japan; and by the Program for Promotion of Fundamental Studies in Health Sciences of the Organization for Pharmaceutical Safety and Research, Tokyo, Japan.

Disclosures

Drs Egashira and Morishita hold a patent on the results reported in the present study. The remaining authors report no conflicts.

References

1. Babapulle MN, Eisenberg MJ. Coated stents for the prevention of restenosis, part I. *Circulation.* 2002;106:2734–2740.
2. Babapulle MN, Eisenberg MJ. Coated stents for the prevention of restenosis, part II. *Circulation.* 2002;106:2859–2866.
3. Virmani R, Farb A, Guagliumi G, Kolodgie FD. Drug-eluting stents: caution and concerns for long-term outcome. *Coron Artery Dis.* 2004;15:313–318.
4. Virmani R, Guagliumi G, Farb A, Musumeci G, Grieco N, Motta T, Mihalcsik L, Tespili M, Valsecchi O, Kolodgie FD. Localized hypersensi-

tivity and late coronary thrombosis secondary to a sirolimus-eluting stent: should we be cautious? *Circulation.* 2004;109:701–705.
5. McFadden EP, Stabile E, Regar E, Cheneau E, Ong AT, Kinnaird T, Suddath WO, Weissman NJ, Torguson R, Kent KM, Pichard AD, Satler LF, Waksman R, Serruys PW. Late thrombosis in drug-eluting coronary stents after discontinuation of antiplatelet therapy. *Lancet.* 2004;364:1519–1521.
6. Carter AJ, Aggarwal M, Kopia GA, Tio F, Tsao PS, Kolata R, Yeung AC, Llanos G, Dooley J, Falotico R. Long-term effects of polymer-based, slow-release, sirolimus-eluting stents in a porcine coronary model. *Cardiovasc Res.* 2004;63:617–624.
7. Farb A, Weber DK, Kolodgie FD, Burke AP, Virmani R. Morphological predictors of restenosis after coronary stenting in humans. *Circulation.* 2002; 105:2974–2980.
8. Egashira K. Molecular mechanisms mediating inflammation in vascular disease: special reference to monocyte chemoattractant protein-1. *Hypertension.* 2003;41:834–841.
9. Ohtani K, Usui M, Nakano K, Kohjimoto Y, Kitajima S, Hirouchi Y, Li XH, Kitamoto S, Takeshita A, Egashira K. Antimonocyte chemoattractant protein-1 gene therapy reduces experimental in-stent restenosis in hypercholesterolemic rabbits and monkeys. *Gene Ther.* 2004;11:1273–1282.
10. Collins T, Cybulsky MI. NF-kappaB: pivotal mediator or innocent bystander in atherogenesis? *J Clin Invest.* 2001;107:255–264.
11. Brand K, Page S, Rogler G, Bartsch A, Brandl R, Knuechel R, Page M, Kaltschmidt C, Baeuerle PA, Neumeier D. Activated transcription factor nuclear factor-kappa B is present in the atherosclerotic lesion. *J Clin Invest.* 1996;97:1715–1722.
12. Landry DB, Couper LL, Bryant SR, Lindner V. Activation of the NF-kappa B and I kappa B system in smooth muscle cells after rat arterial injury: induction of vascular cell adhesion molecule-1 and monocyte chemoattractant protein-1. *Am J Pathol.* 1997;151:1085–1095.
13. Breuss JM, Cejna M, Bergmeister H, Kadl A, Baumgartl G, Steurer S, Xu Z, Koshelnick Y, Lipp J, De Martin R, Losert U, Lammer J, Binder BR. Activation of nuclear factor-kappa B significantly contributes to lumen loss in a rabbit iliac artery balloon angioplasty model. *Circulation.* 2002;105: 633–638.
14. Yamasaki K, Asai T, Shimizu M, Aoki M, Hashiya N, Sakonjo H, Makino H, Kaneda Y, Ogihara T, Morishita R. Inhibition of NFkappaB activation using cis-element 'decoy' of NFkappaB binding site reduces neointimal formation in porcine balloon-injured coronary artery model. *Gene Ther.* 2003;10:356–364.
15. Morishita R, Higaki J, Tomita N, Ogihara T. Application of transcription factor "decoy" strategy as means of gene therapy and study of gene expression in cardiovascular disease. *Circ Res.* 1998;82:1023–1028.
16. Kitamoto S, Egashira K, Kataoka C, Koyanagi M, Katoh M, Shimokawa H, Morishita R, Kaneda Y, Sueishi K, Takeshita A. Increased activity of nuclear factor-kappaB participates in cardiovascular remodeling induced by chronic inhibition of nitric oxide synthesis in rats. *Circulation.* 2000;102:806–812.
17. Takahashi A, Palmer-Opolski M, Smith RC, Walsh K. Transgene delivery of plasmid DNA to smooth muscle cells and macrophages from a biostable polymer-coated stent. *Gene Ther.* 2003;10:1471–1478.
18. van der Giessen WJ, Lincoff AM, Schwartz RS, van Beusekom HM, Serruys PW, Holmes DR Jr, Ellis SG, Topol EJ. Marked inflammatory sequelae to implantation of biodegradable and nonbiodegradable polymers in porcine coronary arteries. *Circulation.* 1996;94:1690–1697.
19. Schwartz RS, Huber KC, Murphy JG, Edwards WD, Camrud AR, Vlietstra RE, Holmes DR. Restenosis and the proportional neointimal response to coronary artery injury: results in a porcine model. *J Am Coll Cardiol.* 1992;19:267–274.
20. Makkar R, Whiting J, Li A, Honda H, Fishbein MC, Knapp FF, Hausleiter J, Litvack F, Eigler NL. Effects of beta(−)-emitting (188)Re balloon in stented porcine coronary arteries: an angiographic, intravascular ultrasound, and histomorphometric study. *Circulation.* 2000;102:3117–3123.
21. Ohtani K, Egashira K, Usui M, Ishibashi M, Hiasa KI, Zhao Q, Aoki M, Kaneda Y, Morishita R, Takeshita A. Inhibition of neointimal hyperplasia after balloon injury by cis-element 'decoy' of early growth response gene-1 in hypercholesterolemic rabbits. *Gene Ther.* 2004;11:126–132.
22. Ohtani K, Egashira K, Hiasa K, Zhao Q, Kitamoto S, Ishibashi M, Usui M, Inoue S, Yonemitsu Y, Sueishi K, Sata M, Shibuya M, Sunagawa K. Blockade of vascular endothelial growth factor suppresses experimental restenosis after intraluminal injury by inhibiting recruitment of monocyte lineage cells. *Circulation.* 2004;110:2444–2452.
23. Lincoff AM, Furst JG, Ellis SG, Tuch RJ, Topol EJ. Sustained local delivery of dexamethasone by a novel intravascular eluting stent to prevent restenosis in the porcine coronary injury model. *J Am Coll Cardiol.* 1997;29:808–816.
24. Egashira K. Clinical importance of endothelial function in arteriosclerosis and ischemic heart disease. *Circ J.* 2002;66:529–533.
25. Griendling KK, FitzGerald GA. Oxidative stress and cardiovascular injury, part II: animal and human studies. *Circulation.* 2003;108:2034–2040.
26. Welt FG, Rogers C. Inflammation and restenosis in the stent era. *Arterioscler Thromb Vasc Biol.* 2002;22:1769–1776.
27. Usui M, Egashira K, Ohtani K, Kataoka C, Ishibashi M, Hiasa K, Katoh M, Zhao Q, Kitamoto S, Takeshita A. Anti-monocyte chemoattractant protein-1 gene therapy inhibits restenotic changes (neointimal hyperplasia) after balloon injury in rats and monkeys. *FASEB J.* 2002;16:1838–1840.
28. Egashira K, Zhao Q, Kataoka C, Ohtani K, Usui M, Charo IF, Nishida K, Inoue S, Katoh M, Ichiki T, Takeshita A. Importance of monocyte chemoattractant protein-1 pathway in neointimal hyperplasia after periarterial injury in mice and monkeys. *Circ Res.* 2002;90:1167–1172.
29. Bellas RE, Lee JS, Sonenshein GE. Expression of a constitutive NF-kappa B-like activity is essential for proliferation of cultured bovine vascular smooth muscle cells. *J Clin Invest.* 1995;96:2521–2527.
30. Lemarie CA, Esposito B, Tedgui A, Lehoux S. Pressure-induced vascular activation of nuclear factor-kappaB: role in cell survival. *Circ Res.* 2003;93: 207–212.
31. Schwartz RS, Edelman ER, Carter A, Chronos N, Rogers C, Robinson KA, Waksman R, Weinberger J, Wilensky RL, Jensen DN, Zuckerman BD, Virmani R. Drug-eluting stents in preclinical studies: recommended evaluation from a consensus group. *Circulation.* 2002;106:1867–1873.
32. Henry SP, Bolte H, Auletta C, Kornbrust DJ. Evaluation of the toxicity of ISIS 2302, a phosphorothioate oligonucleotide, in a four-week study in cynomolgus monkeys. *Toxicology.* 1997;120:145–155.
33. Suzuki J, Ito H, Goto R, Morishita R, Egashira K, Isobe M. Initial clinical cases of the use of a NF-kappaB decoy at the site of coronary stenting for the prevention of restenosis. *Circ J.* 2004;68:270–271.

CLINICAL PERSPECTIVE

Although first-generation drug-eluting stents are effective in reducing the rate of restenosis, the drug-eluting stent has no effect on the incidence of cardiovascular events compared with the bare-metal stent. In addition, recent clinical studies have demonstrated that drug-eluting stents increase the incidence of late stent thrombosis, leading to acute myocardial infarction and death after the discontinuation of clopidogrel. These serious late thrombotic events are thought to result from impaired endothelial regeneration and an incomplete healing process because of the drugs or polymers used in the construction of drug-eluting stents. Therefore, the formulation of a novel drug-eluting stent system with fewer adverse effects is warranted. In the present study, we formulate a nuclear factor-κB (NF-κB) decoy–eluting stent with biocompatible polymer technology and report inhibition of neointimal formation by stent-based delivery of NF-κB decoy. Importantly, no histopathological evidence of impaired endothelial regeneration and healing process was noted at sites of stents coated with polymer alone and polymer plus decoy. These data support the experimental evidence that the NF-κB decoy–eluting stent is effective in reducing in-stent neointimal formation and thrombosis. Our previous clinical trial testing the feasibility and safety of NF-κB decoy supports the notion that this NF-κB decoy–eluting stent system can be applied to the clinical setting. Ultimately, we propose that this system be used to treat vulnerable plaques leading to acute coronary syndrome and stroke.

Angiotensin II Type 1 Receptor Blocker Attenuates Exacerbated Left Ventricular Remodeling and Failure in Diabetes–Associated Myocardial Infarction

Hidenori Matsusaka, MD, PhD, Shintaro Kinugawa, MD, PhD,† Tomomi Ide, MD, PhD,* Shouji Matsushima, MD,* Tetsuya Shiomi, MD, PhD,* Toru Kubota, MD, PhD,* Kenji Sunagawa, MD, PhD,* and Hiroyuki Tsutsui, MD, PhD†*

Abstract: Diabetes mellitus adversely affects the outcomes in patients with myocardial infarction (MI), due in part to the exacerbation of left ventricular (LV) remodeling. Although angiotensin II type 1 receptor blocker (ARB) has been demonstrated to be effective in the treatment of heart failure, information about the potential benefits of ARB on advanced LV failure associated with diabetes is lacking. To induce diabetes, male mice were injected intraperitoneally with streptozotocin (200 mg/kg). At 2 weeks, anterior MI was created by ligating the left coronary artery. These animals received treatment with olmesartan (0.1 mg/kg/day; n = 50) or vehicle (n = 51) for 4 weeks. Diabetes worsened the survival and exaggerated echocardiographic LV dilatation and dysfunction in MI. Treatment of diabetic MI mice with olmesartan significantly improved the survival rate (42% versus 27%, $P < 0.05$) without affecting blood glucose, arterial blood pressure, or infarct size. It also attenuated LV dysfunction in diabetic MI. Likewise, olmesartan attenuated myocyte hypertrophy, interstitial fibrosis, and the number of apoptotic cells in the noninfarcted LV from diabetic MI. Post-MI LV remodeling and failure in diabetes were ameliorated by ARB, providing further evidence that angiotensin II plays a pivotal role in the exacerbated heart failure after diabetic MI.

Key Words: myocardial infarction, diabetes mellitus, heart failure, remodeling, apoptosis

(*J Cardiovasc Pharmacol*™ 2006;48:95–102)

INTRODUCTION

Diabetes mellitus (DM) is one of the largest comorbidities of patients with acute myocardial infarction (MI). Diabetic patients who have had MI have a higher incidence of death than do nondiabetic patients, both in the acute phase and on long-term follow-up.[1] The excess mortality of diabetic patients results primarily from the development of heart failure and recurrent MI.[2] MI frequently produces progressive left ventricular (LV) dilatation associated with hypertrophy of noninfarcted LV. These changes in LV geometry, referred to as remodeling, contribute to the development of depressed cardiac function.[3] Several mechanisms, whether alone or in combination, may adversely affect LV remodeling and failure after MI in diabetic patients; such mechanisms include severe coronary artery disease, impaired vasodilatory reserve of coronary arteries, and preexisting LV dysfunction due to diabetic cardiomyopathy.[4] Clinical studies in patients with acute MI showed that the mortality is higher in diabetic patients despite similar coronary patency rates, suggesting that the exacerbation of LV dysfunction after MI in the presence of DM may play a major role.[5] In fact, our recent experimental studies demonstrated that the streptozotocin (STZ)–induced hyperglycemia exacerbated the progressive LV chamber dilatation and contractile dysfunction in a murine model of MI.[6] In diabetic MI mice, myocyte hypertrophy and apoptosis in association with interstitial fibrosis were more enhanced in diabetic post-MI hearts. We thus considered that these remodeling processes might be mutually reinforcing in the setting of MI associated with diabetes, and DM may further enhance the development of heart failure.

Angiotensin-converting enzyme (ACE) inhibitors and angiotensin II (AngII) type 1 receptor blockers (ARBs) have been shown to decrease the mortality and morbidity of patients with MI and heart failure.[7–9] Experimental evidence indicates that these drugs are effective in limiting post-MI LV remodeling and failure.[10–12] Moreover, ACE inhibitors and ARBs have been demonstrated to prevent or retard the development of diabetic complications including both microangiopathy and macroangiopathy.[13,14]

It has not yet been determined, however, whether AngII plays a key role in the exacerbation of post-MI failure in the

Received for publication June 7, 2006; accepted August 5, 2006.
From the *Department of Cardiovascular Medicine, Graduate School of Medical Sciences, Kyushu University, Fukuoka; and the †Department of Cardiovascular Medicine, Hokkaido University Graduate School of Medicine, Sapporo, Japan.
This study was supported in part by grants from the Ministry of Education, Science, and Culture (No. 12670676, 14370230, 17390223, 17659223) and SANKYO CO., LTD.
Reprints: Hiroyuki Tsutsui, MD, PhD, Department of Cardiovascular Medicine, Hokkaido University Graduate School of Medicine, Kita-15, Nishi-7, Kita-ku, Sapporo 060-8638, Japan (e-mail: htsutsui@med.hokudai.ac.jp).

presence of DM. The present study was thus performed to determine the effects of an ARB on the accelerated LV remodeling after MI associated with DM. Furthermore, various cellular and molecular mechanisms were evaluated to further elucidate critical pathways implicated in this model and in mediating cardiac protection by ARBs in diabetes-associated post-MI LV remodeling.

METHODS

Experimental Design

The study was approved by our Institutional Animal Research Committee and conformed to the animal care guidelines of the American Physiological Society.

DM was induced in male CD-1 mice (5–7 weeks old; 25-35 g body weight) by intraperitoneal injection of STZ (200 mg/kg body weight).[6] Tail vein blood glucose was measured 5 days after injection to ensure induction of diabetes. As a control, vehicle (0.1 mol/L citrate buffer, pH 4.5) was injected in another group of mice. At 2 weeks after injection, MI was created in STZ-injected mice (DM-MI group) by ligating the left coronary artery.[6] After the creation of MI, these animals were further randomized to be treated with an ARB, olmesartan (0.1 mg /kg body weight/day in osmotic minipump, SANKYO; DM-MI+Olmesartan group) or to receive vehicle (DM-MI+Vehicle group). Sham operation without ligating the coronary artery was also performed (Control groups), and these animals were also randomized to be treated with olmesartan or to receive vehicle.

All 4 groups of mice (Control+Vehicle, n = 11; Control+Olmesartan, n = 11; DM-MI+Vehicle, n = 51; DM-MI+Olmesartan, n = 50) were followed for further 4 weeks (Fig. 1).

Survival

During the study period of 6 weeks (2 weeks after vehicle or STZ injection and further 4 weeks after surgery), cages were inspected daily for deceased animals. All deceased mice were examined for the presence of pleural effusion and cardiac rupture.

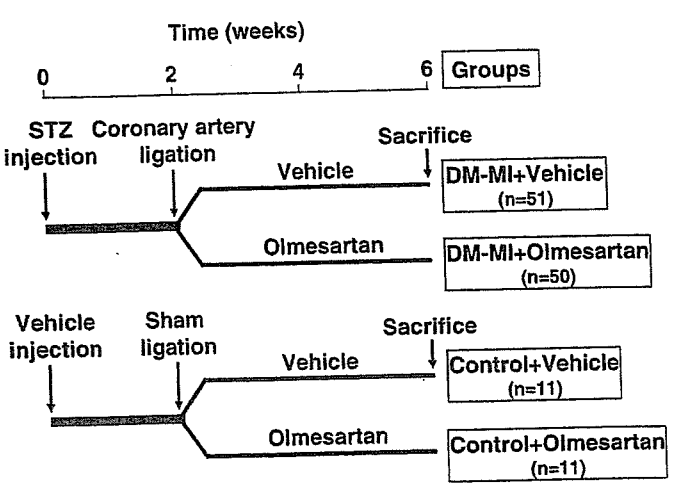

FIGURE 1. Experimental protocol. STZ, streptozotocin; DM, diabetes mellitus; MI, myocardial infarction.

Blood Glucose

Before sacrifice, venous blood samples (0.5 mL) were collected for determination of blood glucose levels.

Echocardiography and Hemodynamics

Echocardiographic studies were performed under light anesthesia with tribromoethanol/amylene hydrate (Avertin; 2.5% wt/vol, 8 μL/g intraperitoneally) and spontaneous respiration. A 2-dimensional parasternal short-axis view of the LV was obtained at the level of the papillary muscles. In general, the best views were obtained with the transducer lightly applied to the mid upper left anterior chest wall. The transducer was then gently moved cephalad or caudad and angulated until desirable images were obtained. After it was ensured that the imaging was on axis (on the basis of LV cavity roundness), two-dimensional targeted M-mode tracings were recorded at a paper speed of 50 mm/sec. Under the same anesthesia with Avertin, a 1.4 French micromanometer-tipped catheter (Millar Instruments) was inserted into the right carotid artery and then advanced into the LV to measure LV pressures.[6] One subset of investigators, who were not informed of the experimental groups, performed in vivo LV function studies.

Our validation study confirmed that the intraobserver and interobserver variabilities for our echocardiographic measurements of LV dimensions and fractional shortening were excellent, and the measurements made in the same animals on separate days were highly reproducible.[15]

Tissue Preparation and Morphometric Analysis

The heart was excised and dissected into the right and left ventricles, including the septum. The left ventricle was cut into 3 transverse sections; apex, middle ring, and base. From the middle ring, 5-μm sections were cut and stained with Masson's trichrome. The boundary lengths of the infarcted and noninfarcted endocardial and epicardial surfaces were traced with a planimeter digital image analyzer.

Infarct size (fraction of the infarcted LV) was calculated as the average of all slices and expressed as the percentage of length of circumference.[6] Myocyte cross-sectional area and collagen volume fraction were determined by quantitative morphometry of tissue sections from mid-LV.[6]

Myocardial AngII Type 1 (AT1) Receptor

The myocardial tissues with MI were carefully dissected into 3 parts: the infarcted LV, the border zone LV with the peri-infarct rim (a 1-mm rim of normal-appearing tissue), and the remaining noninfarcted (remote) LV. Total RNA was extracted from each sample by the acid guanidinium thiocyanate-phenol-chloroform method (ISOGEN, Nippon Gene).[16] Myocardial AT_1 receptor gene expression was analyzed by real-time quantitative reverse transcription–polymerase chain reaction (RT-PCR) with the use of the TaqMan system on the basis of real-time detection of accumulated fluorescence (ABI Prism 7000, Applied Biosystems) and was normalized in relation to the expression of an endogenous control, glyceraldehydes-3-phosphate-dehydrogenase (GAPDH).

Myocardial TGF-β and MMPs/TIMPs

Transforming growth factor-β (TGF-β) and matrix metalloproteinases (MMPs), including MMP-1, -2, -3, -8, and -9, as well as tissue inhibitors of MMPs (TIMPs), including TIMP-1, -2, -3, and -4, mRNA levels were determined by multiprobe ribonuclease protection assay (RPA, RiboQuant, PharMingen) according to the methods described previously.[17] Each value was normalized to that of GAPDH in each template set as an internal control, followed by calculation as a ratio to Control+Vehicle.

Apoptosis

Tissue sections from the mid-LV were stained with terminal deoxynucleotidyl transferase-mediated dUTP nick end-labeling (TUNEL) staining.[6] Staining with hematoxylin was carried out on the same section for visualization of nuclei. The number of TUNEL-positive nuclei was counted, and the data were normalized per 10^5 total nuclei identified by hematoxylin-positive staining in the same sections. The proportion of apoptotic cells was counted in the noninfarcted LV.

We further examined whether apoptosis is present in the noninfarcted LV by the more sensitive ligation-mediated PCR fragmentation assays (Maxim Biotech).

Statistical Analyses

Data are expressed as means ± SEM. Comparison of survival was performed by the Kaplan-Meier analysis. For multiple-group comparisons, ANOVA followed by Bonferroni's t test was performed. $P < 0.05$ was considered statistically significant.

RESULTS

We employed 4 groups of Control+Vehicle (n = 11), Control+Olmesartan (n = 11), DM-MI+Vehicle (n = 51), and DM-MI+Olmesartan (n = 50) mice in the present study. The survival analysis was performed in all of these mice. Subsequent echocardiographic and hemodynamic measurements were performed in the 6-week survivors; 11 Control+Vehicle, 11 Control+Olmesartan, 14 DM-MI+Vehicle, and 21 DM-MI+Olmesartan mice. These measurements could not be accomplished in 2 DM-MI+Vehicle and 9 DM-MI+Olmesartan mice due to the technical difficulties. The surviving mice were further divided into 2 groups; those for the subsequent histological analysis, including infarct size, myocyte cross-sectional area, and collagen volume fraction as well as TUNEL staining (5 Control+Vehicle, 5 Control+Olmesartan, 5 DM-MI+Vehicle, and 5 DM-MI+Olmesartan), and those for the biochemical assay including TGF-β and MMPs/TIMPs (6 Control+Vehicle, 6 Control+Olmesartan, 8 DM-MI+Vehicle, and 8 DM-MI+Olmesartan).

Survival and Blood Glucose

The mortality rates during 24 hours after ligation were 15% and 19% in DM-MI+Vehicle and DM-MI+Olmesartan mice, respectively (P = NS). Survival rates during the study period were significantly higher in DM-MI+Olmesartan than in DM-MI+Vehicle (Fig. 2). Death was suspected to be attributable to heart failure and/or arrhythmia. A single DM+MI+Vehicle (2%) and 1 DM-MI+Olmesartan (2%) mice died from LV rupture (P = NS).

Blood glucose levels at 5 days as well as 6 weeks after injection were significantly higher in the diabetic mice than in the nondiabetic mice, but they were not significantly different between DM-MI+Vehicle and DM-MI+Olmesartan mice (Table 1).

Echocardiography and Hemodynamics

In comparison with control mice, DM-MI mice showed LV dilatation and dysfunction by echocardiography, both of which were significantly ameliorated in DM-MI+Olmesartan mice (Fig. 3 and Table 1).

Heart rate was comparable among all groups (Table 1). Mean aortic blood pressure was lower in DM-MI groups than in the control groups, but there was no significant difference between DM-MI+Vehicle and DM-MI+Olmesartan. LV end-diastolic pressure (EDP) was increased in DM-MI+Vehicle mice and was significantly reduced in DM-MI+Olmesartan mice. LV dP/dt_{max} was decreased in DM+MI groups and tended to be higher in DM+MI-Olmesartan than in DM-MI+Vehicle but did not reach statistical significance (P = 0.09).

Organ Weights

Body weight was lower in DM-MI mice (Table 1), as previously observed.[6] In contrast, the tibial length was similar among all groups. Coinciding with an increased LV EDP, lung weight/tibial length was increased in the DM-MI groups, and this increase was significantly attenuated by olmesartan. The

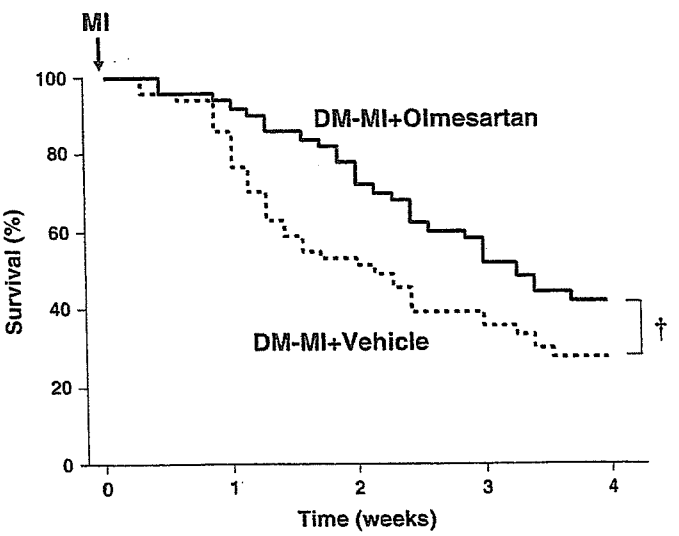

FIGURE 2. Kaplan-Meier survival analysis. Percentages of surviving DM-MI+Vehicle (n = 51) and DM-MI+Olmesartan (n = 50) mice were plotted. Overall survival was significantly higher in DM-MI+Olmesartan than in DM-MI+Vehicle. †$P <$ 0.01 for difference from the DM-MI+Vehicle group.

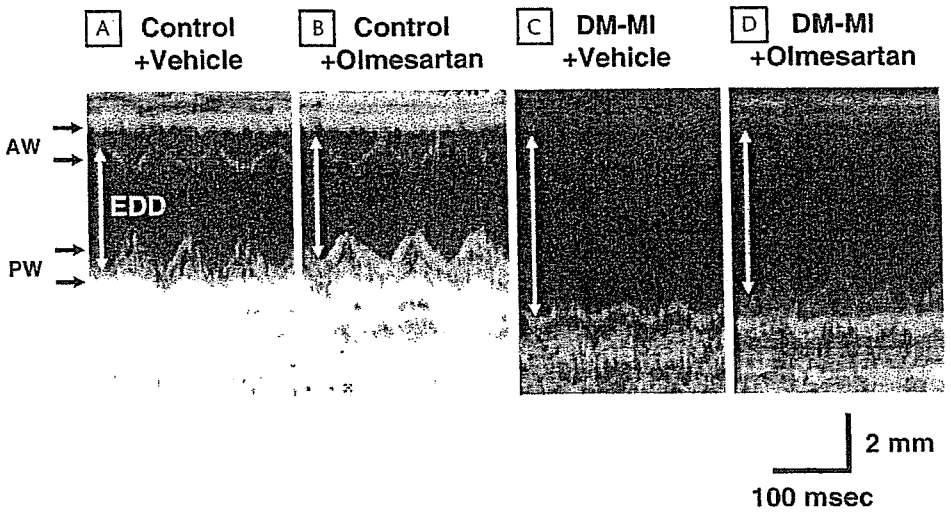

FIGURE 3. M-mode echocardiograms obtained from Control+Vehicle (A), Control+Olmesartan (B), DM-MI+Vehicle (C), and DM-MI+Olmesartan (D) 4 weeks after surgery. AW, anterior wall; PW, posterior wall; EDD, end-diastolic diameter.

prevalence of pleural effusion was significantly lower in DM-MI+Olmesartan than in DM-MI+Vehicle.

Infarct Size

Infarct size determined by the histomorphometric analysis of LV sections was comparable (61 ± 4% versus 59 ± 2%; P = NS) between DM-MI+Vehicle (n = 5) and DM-MI+Olmesartan (n = 5).

Histomorphometry

Myocyte cross-sectional area was significantly increased in DM-MI groups compared with control groups (Fig. 4).

TABLE 1. Blood Chemistry, Echocardiography, Hemodynamics, and Organ Weights

	Control+Vehicle	Control+Olmesartan	DM-MI+Vehicle	DM-MI+Olmesartan
Blood chemistry				
n	11	11	51	50
Blood glucose at 5 days, mg/dl	104 ± 5	109 ± 7	377 ± 9‡	380 ± 9‡
n	11	11	14	21
Blood glucose at 6 weeks, mg/dl	112 ± 5	120 ± 3	445 ± 28‡	473 ± 15‡
Echocardiography				
n	11	11	13	19
Heart rate, bpm	477 ± 9	475 ± 7	480 ± 7	483 ± 6
LVEDD, mm	4.0 ± 0.1	4.0 ± 0.1	6.0 ± 0.2‡	5.6 ± 0.1‡
LVESD, mm	2.6 ± 0.1	2.5 ± 0.1	5.3 ± 0.2‡	4.9 ± 0.1‡§
Ejection fraction, %	74.3 ± 0.9	75.7 ± 0.7	30.6±1.7 ‡	35.6 ± 1.3‡§
Hemodynamics				
n	11	11	12	12
Heart rate, bpm	453 ± 10	443 ± 13	467 ± 14	478 ± 8
Systolic blood pressure, mmHg	93 ± 2	93 ± 2	85 ± 2†	78 ± 2‡
$LVdP/dt_{max}$, mmHg/sec	10874 ± 684	11548 ± 601	4425 ± 431‡	5664 ± 389‡
$LVdP/dt_{min}$, mmHg/sec	8555 ± 537	8576 ± 314	2836 ± 230‡	3365 ± 194‡
LVEDP, mmHg	1.0 ± 0.5	1.2 ± 0.6	23.3 ± 1.7‡	13.0 ± 1.8‡¶
Organ weights				
n	11	11	14	21
Body wt, g	35.1 ± 0.9	35.3 ± 0.9	28.2 ± 1.1‡	29.2 ± 1.1‡
TL, mm	20.6 ± 0.8	20.3 ± 0.9	21.1 ± 0.1	21.2 ± 0.1
LV wt/TL, mg/mm	3.7 ± 0.3	3.6 ± 0.1	3.3 ± 0.1	3.1 ± 0.1*
Lung wt/TL, mg/mm	7.2 ± 0.3	7.7 ± 0.2	16.0 ± 1.4‡	12.3 ± 1.0‡§
Pleural effusion, %	—	—	86	48§

Values are means ± SEM.
†$P < 0.05$ vs. Control+Vehicle.
‡$P < 0.01$ vs. Control+Vehicle.
§$P < 0.05$ vs. DM-MI+Vehicle.
¶$P < 0.01$ vs. DM-MI+Vehicle.
LV, left ventricular; EDD, end-diastolic diameter; ESD, end-systolic diameter; EDP, end-diastolic pressure; wt, weight; TL, tibial length.

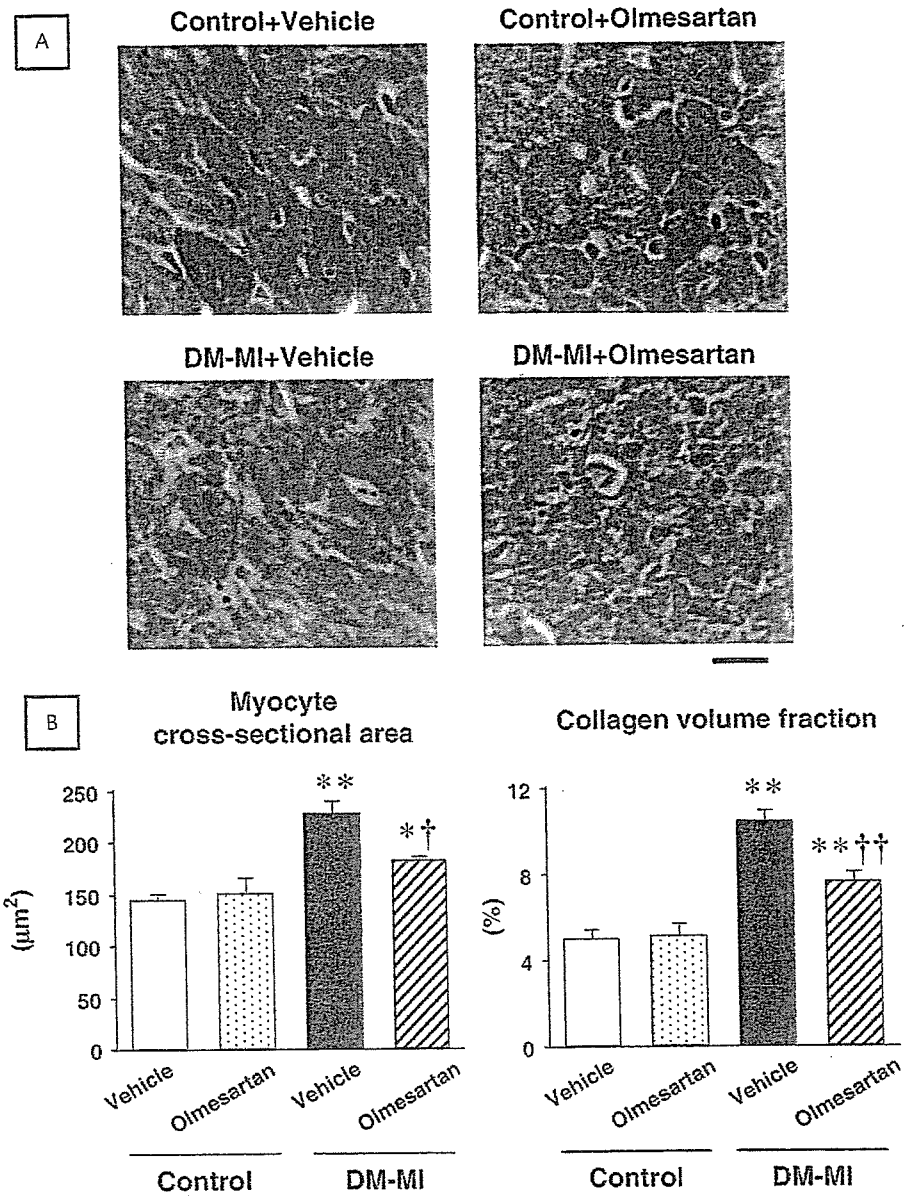

FIGURE 4. (A) Representative light microscopic photomicrographs of Masson's trichrome-stained myocardial sections obtained from Control+Vehicle, Control+Olmesartan, DM-MI+Vehicle, and DM-MI+Olmesartan mice. Scale bar represents 10 μm. (B) Summarized data for myocyte cross-sectional area and collagen volume fraction from Control+Vehicle, Control+Olmesartan, DM-MI+Vehicle, and DM-MI+Olmesartan (n = 5 for each) mice. Values are means ± SEM. $*P < 0.05$, $**P < 0.01$ for difference from the Control+Vehicle value. $\dagger P < 0.05$, $\dagger\dagger P < 0.01$ for difference from the corresponding DM-MI+Vehicle value.

Collagen volume fraction was also increased in DM-MI groups. Both of this increase was significantly ameliorated in DM-MI+Olmesartan (Fig. 4).

Myocardial AT_1 receptor

AT_1 receptor gene expression was 1.9-fold increased in the LV from DM-MI mice compared to control mice ($P < 0.05$).

TGF-ß and MMPs/TIMPs

TGF-ß mRNA was significantly increased in DM-MI+Vehicle, and this increase was attenuated in DM-MI+Olmesartan (Fig. 5).

MMP-2 mRNA levels significantly increased in the DM-MI compared with control mice (Fig. 6). This increase was significantly attenuated in DM-MI+Olmesartan. Other MMPs, including MMP-1, -3, -8, and -9, were not altered in these mice (Fig. 6). The changes of TIMPs (TIMP-1, -2, -3, and -4) were also comparable between DM-MI+Vehicle and DM-MI+Olmesartan.

Apoptosis

There were rare TUNEL-positive nuclei in control mice. The number of TUNEL-positive cells in the noninfarcted LV was increased in the DM-MI groups. It decreased in DM-MI+Olmesartan compared with DM-MI+Vehicle (Fig. 7A). In addition, the intensity of DNA ladder indicated that the apoptosis in the noninfarcted LV from DM-MI+Olmesartan was attenuated compared with DM-MI+Vehicle (Fig. 7B).

DISCUSSION

In the presence of DM, MI mice had poor survival, decreased overall LV ejection performance, and exacerbated

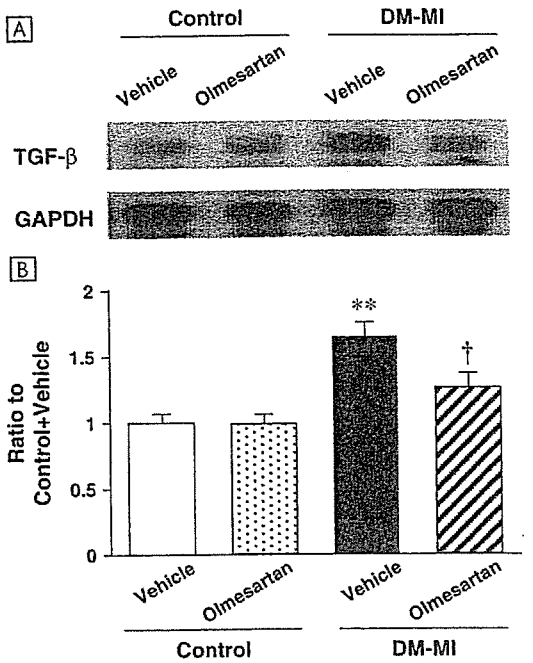

FIGURE 5. (A) Representative image of myocardial gene expression of TGF-β. (B) Densitometric analysis of TGF-β gene expression in Control+Vehicle (n = 6), Control+Olmesartan (n = 6), DM-MI+Vehicle (n = 8), and DM-MI+Olmesartan (n = 8) mice. Data were normalized by GAPDH concurrently run on the same gel and expressed as the ratio to Control+Vehicle values. Values are means ± SEM. $^{**}P < 0.01$ for difference from the Control+Vehicle value. $\dagger P < 0.05$ for difference from the corresponding DM-MI+Vehicle value.

LV remodeling, increased chamber dilatation as well as myocyte apoptosis and interstitial fibrosis of the noninfarcted myocardium, all of which were significantly ameliorated by the treatment of MI mice with olmesartan. Therefore, AngII may play a pivotal role in the development and exacerbation of heart failure after MI associated with diabetes.

Impact of DM in Post-MI LV Remodeling

MI leads to complex structural alterations (remodeling) involving both the infarcted and noninfarcted myocardium. Early remodeling is LV cavity dilatation occurring during the early phase of MI, which is likely due to wall thinning of the infarct region. During the first several days, LV enlargement follows; thereafter, a progressive dilatation of the noninfarcted LV associated with myocyte hypertrophy and interstitial fibrosis occurs over weeks. These progressive changes in LV geometry contribute to the development of depressed cardiac function, clinical heart failure, and increased mortality. Our recent study has demonstrated that hyperglycemia per se exacerbates post-MI LV remodeling and failure.[6] In diabetic MI mice, myocyte hypertrophy and apoptosis in association with interstitial fibrosis were more enhanced in diabetic post-MI hearts. These results indicate that post-MI remodeling processes might be mutually reinforcing in the setting of MI associated with DM, and DM may further enhance the development of heart failure. This may explain, at least in part, the clinical findings that the outcome after MI in diabetic patients is worse than that in nondiabetic patients.[1,2,5]

Effects of ARB on Post-MI Remodeling and Failure with DM

Accumulating evidence suggests that the cardiac renin-angiotensin system (RAS) is activated during the development and progression of LV remodeling and failure after MI[18] and that ACE inhibitors and ARBs have the favorable effects on these deleterious processes.[11,19] In addition, recent studies have shown that the RAS is activated also in DM.[20] Therefore, the combination of DM and MI together may synergistically activate the RAS in the heart, which may further damage its function and

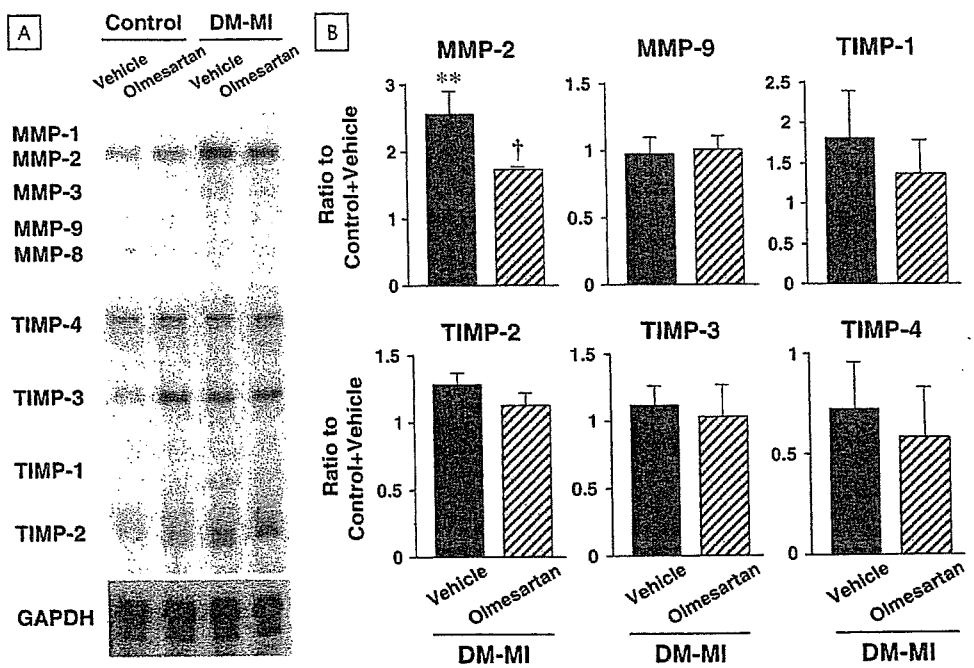

FIGURE 6. (A) Representative images of myocardial gene expression of MMPs/TIMPs. (B) Densitometric analysis of MMP and TIMP gene expression from DM-MI+Vehicle (n = 4) and DM-MI+Olmesartan (n = 4) mice. Each value was normalized to that of GAPDH in each template set as an internal control and expressed as the ratio to Control+Vehicle (n = 4). Values are means ± SEM. $^{**}P < 0.01$ for difference from the Control+Vehicle values. $\dagger P < 0.05$ for difference from the corresponding DM-MI+Vehicle values.

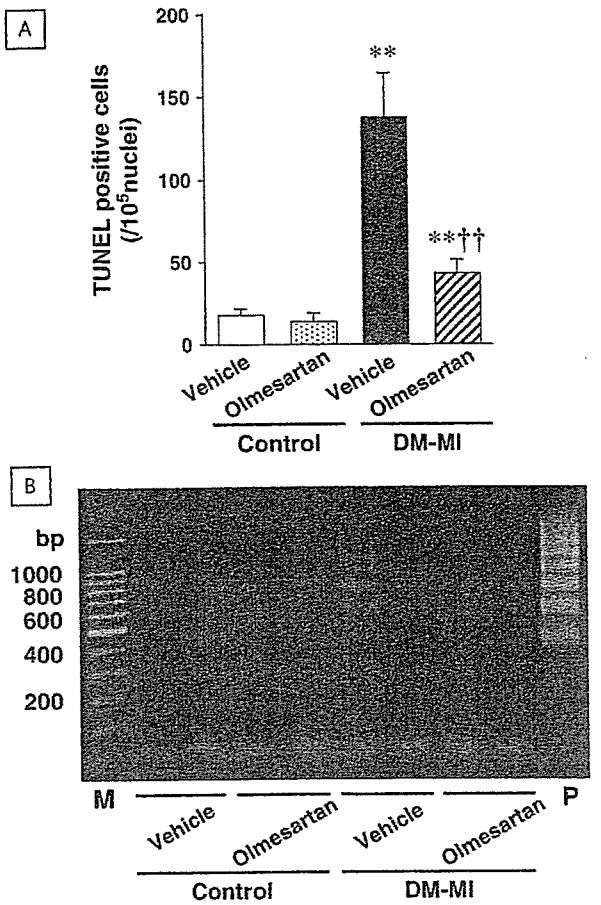

FIGURE 7. (A) The number of TUNEL-positive cells in the noninfarcted LV from Control+Vehicle, Control+Olmesartan, DM-MI+Vehicle, and DM-MI+Olmesartan (n = 5 for each) mice. Values are means ± SEM. $^{**}P < 0.01$ for difference from the Control+Vehicle values. $^{††}P < 0.01$ for difference from the corresponding DM-MI+Vehicle values. (B) DNA ladder indicative of apoptosis was detectable in the genomic DNA from the noninfarcted LV. M, 100 bp DNA ladder markers; P, positive control.

structure.[21] However, the beneficial effects of ACE inhibitors or ARBs in the context of diabetic MI have not been previously investigated. The present study clearly demonstrates that the post-MI LV remodeling and failure in DM were ameliorated by olmesartan, providing further evidence that AngII plays a pivotal role in the exacerbated heart failure after MI with diabetes.

Mechanisms of Beneficial Effects by ARB

There may be several factors attributable to the protective effects conferred by olmesartan on post-MI remodeling and failure. They were not due to its MI size-sparing effects because the infarct size was comparable between DM-MI+Vehicle and DM-MI+Olmesartan mice (Table 1). Further, its effects were not attributable to those on glycemic control. More importantly, they were independent of hemodynamics because blood pressure and heart rate were not altered (Table 1). Diabetes-induced acceleration of post-MI LV remodeling was associated with a significant increase in myocyte hypertrophy and interstitial fibrosis. The improved LV function by olmesartan was associated with a significant decrease in these hypertrophic and fibrotic changes in the noninfarcted LV (Fig. 4). One proposed mechanism by olmesartan for inhibiting LV structure alterations in DM-MI is related to a decrease in TGF-β expression and the resultant amelioration of cardiac fibrosis by olmesartan (Fig. 5). TGF-β is a locally generated cytokine that has been implicated as a major stimulator of tissue fibrosis. It has a major influence on fibroblast proliferation and extracellular matrix (ECM) production, particularly of collagen and fibronectin, while reducing degradation of these components. Because TGF-β is one of growth factors that influence tissue repair and remodeling, its activation might be well expected to play an important role in LV structural changes after MI. Olmesartan might directly ameliorate the increased expression of myocardial TGF-β expression in DM-MI mice because AngII is a well-known mediator to induce and activate TGF-β.[22] Another possible mechanism is the attenuation of myocardial MMP-2 expression in DM-MI+Olmesartan mice. It has been reported that myocardial MMPs are increased in MI.[23] Further, the inhibition of MMPs has been shown to limit the chamber remodeling after MI.[23] Therefore, MMP activation might play an important role in the pathophysiology of LV remodeling. Myocardial MMPs can be activated by AngII.[24] On the basis of these findings, the activation of myocardial RAS could contribute to the activation of myocardial MMP-2 and thus to the development of LV remodeling. Finally, recent studies have demonstrated that apoptosis is thought to contribute to the progressive deterioration of LV function after MI. Previous studies have demonstrated that apoptosis appears in not only infarcted but also noninfarcted myocardium after MI.[25] Specifically, apoptosis occurs in the noninfarcted LV late after MI. This is an intriguing observation in light of the remodeling process known to occur within the noninfarcted area, which is characterized by loss of myocytes, hypertrophy of remaining myocytes, and interstitial replacement fibrosis. In fact, recent studies have suggested that cardiac myocyte apoptosis contributes to LV remodeling after MI.[26,27] Moreover, AngII can mediate myocyte apoptosis, which may lead to myocardial remodeling and failure. Therefore, in DM-MI mice, olmesartan could directly ameliorate apoptosis and eventual post-MI cardiac failure.

Limitations

First, the present study could not elucidate the mechanism of death, arrhythmias or depressed cardiac function, because the telemetry of electrocardiograms was not performed. More importantly, it remains uncertain whether the beneficial effects of ARB could be attributable to the reduction of arrhythmic or heart failure death. Second, we used only olmesartan and did not examine the effects of other ARBs or ACE inhibitors in the present study. Therefore, we could not comment whether our findings are specific for olmesartan or other ARBs and ACE inhibitors could provide similar beneficial effects. Third, the changes in ECM synthesis/degradation diversely affect LV remodeling among different sites within the LV. However, we performed the biochemical analysis only in the noninfarcted LV from MI mice because the amount of tissue was very limited in the infarcted and border zone LV. Moreover, the molecular and biochemical alterations of ECM

especially at the noninfarcted LV are involved in the development and progression of post-MI remodeling and failure.

Clinical Implications

A number of clinical studies have reported that the prognosis after MI is worse in diabetic patients because they exhibit a higher incidence of heart failure and death compared with nondiabetic patients.[4] This may be due to the concomitant presence of severe coronary atherosclerotic lesions in diabetic patients. However, both experimental and clinical studies have shown that DM causes a specific form of myocardial damage independent of coronary atherosclerosis and manifests itself as LV dysfunction.[28] In addition to an acceleration of coronary atherosclerosis and an impairment of collateral formation, diabetes-induced exacerbation of LV remodeling and failure after MI is an important pathogenic mechanism responsible for this phenomenon.[6] The findings in the present study may further draw attention to the early and intensive treatment of heart failure by using ACE inhibitors or ARBs in diabetic patients with MI. Clinical evidence has further confirmed that these drugs improve the mortality and morbidity of patients with MI and heart failure.[7,8,29]

CONCLUSIONS

In the presence of diabetes, the cardiac RAS may mediate the acceleration of post-MI LV remodeling, and the inhibition of this system may reduce the diabetes-associated exacerbation of post-MI LV remodeling and failure.

ACKNOWLEDGMENTS

This study was supported in part by grants from the Ministry of Education, Science and Culture (No. 12670676, 14370230, 17390223, 17659223) and SANKYO CO., LTD. A part of this study was conducted in Kyushu University Station for Collaborative Research II.

REFERENCES

1. Haffner SM, Lehto S, Ronnemaa T, et al. Mortality from coronary heart disease in subjects with type 2 diabetes and in nondiabetic subjects with and without prior myocardial infarction. *N Engl J Med.* 1998;339:229–234.
2. Woodfield SL, Lundergan CF, Reiner JS, et al. Angiographic findings and outcome in diabetic patients treated with thrombolytic therapy for acute myocardial infarction: the GUSTO-I experience. *J Am Coll Cardiol.* 1996; 28:1661–1669.
3. Pfeffer MA, Braunwald E. Ventricular remodeling after myocardial infarction. Experimental observations and clinical implications. *Circulation.* 1990;81:1161–1172.
4. Stone PH, Muller JE, Hartwell T, et al. The effect of diabetes mellitus on prognosis and serial left ventricular function after acute myocardial infarction: contribution of both coronary disease and diastolic left ventricular dysfunction to the adverse prognosis. The MILIS Study Group. *J Am Coll Cardiol.* 1989;14:49–57.
5. Granger CB, Califf RM, Young S, et al. Outcome of patients with diabetes mellitus and acute myocardial infarction treated with thrombolytic agents. The Thrombolysis and Angioplasty in Myocardial Infarction (TAMI) Study Group. *J Am Coll Cardiol.* 1993;21:920–925.
6. Shiomi T, Tsutsui H, Ikeuchi M, et al. Streptozotocin-induced hyperglycemia exacerbates left ventricular remodeling and failure after experimental myocardial infarction. *J Am Coll Cardiol.* 2003;42:165–172.
7. Pfeffer MA, Braunwald E, Moye LA, et al. Effect of captopril on mortality and morbidity in patients with left ventricular dysfunction after myocardial infarction. Results of the survival and ventricular enlargement trial. The SAVE Investigators. *N Engl J Med.* 1992;327:669–677.
8. Dickstein K, Kjekshus J. Effects of losartan and captopril on mortality and morbidity in high-risk patients after acute myocardial infarction: the OPTIMAAL randomised trial. Optimal Trial in Myocardial Infarction with Angiotensin II Antagonist Losartan. *Lancet.* 2002;360:752–760.
9. Pfeffer MA, McMurray JJ, Velazquez EJ, et al. Valsartan, captopril, or both in myocardial infarction complicated by heart failure, left ventricular dysfunction, or both. *N Engl J Med.* 2003;349:1893–1906.
10. Schieffer B, Wirger A, Meybrunn M, et al. Comparative effects of chronic angiotensin-converting enzyme inhibition and angiotensin II type 1 receptor blockade on cardiac remodeling after myocardial infarction in the rat. *Circulation.* 1994;89:2273–2282.
11. Yoshiyama M, Takeuchi K, Omura T, et al. Effects of candesartan and cilazapril on rats with myocardial infarction assessed by echocardiography. *Hypertension.* 1999;33:961–968.
12. Mankad S, d'Amato TA, Reichek N, et al. Combined angiotensin II receptor antagonism and angiotensin-converting enzyme inhibition further attenuates postinfarction left ventricular remodeling. *Circulation.* 2001;103:2845–2850.
13. Cooper ME. Pathogenesis, prevention, and treatment of diabetic nephropathy. *Lancet.* 1998;352:213–219.
14. Effects of ramipril on cardiovascular and microvascular outcomes in people with diabetes mellitus: results of the HOPE study and MICRO-HOPE substudy. Heart Outcomes Prevention Evaluation Study Investigators. *Lancet.* 2000;355:253–259.
15. Shiomi T, Tsutsui H, Hayashidani S, et al. Pioglitazone, a peroxisome proliferator-activated receptor-gamma agonist, attenuates left ventricular remodeling and failure after experimental myocardial infarction. *Circulation.* 2002;106:3126–3132.
16. Usui M, Egashira K, Tomita H, et al. Important role of local angiotensin II activity mediated via type 1 receptor in the pathogenesis of cardiovascular inflammatory changes induced by chronic blockade of nitric oxide synthesis in rats. *Circulation.* 2000;101:305–310.
17. Matsusaka H, Ikeuchi M, Matsushima S, et al. Selective disruption of MMP-2 gene exacerbates myocardial inflammation and dysfunction in mice with cytokine-induced cardiomyopathy. *Am J Physiol Heart Circ Physiol.* 2005;289:H1858–1864.
18. Yamagishi H, Kim S, Nishikimi T, et al. Contribution of cardiac renin-angiotensin system to ventricular remodelling in myocardial-infarcted rats. *J Mol Cell Cardiol.* 1993;25:1369–1380.
19. Liu YH, Yang XP, Sharov VG, et al. Effects of angiotensin-converting enzyme inhibitors and angiotensin II type 1 receptor antagonists in rats with heart failure. Role of kinins and angiotensin II type 2 receptors. *J Clin Invest.* 1997;99:1926–1935.
20. Fiordaliso F, Li B, Latini R, et al. Myocyte death in streptozotocin-induced diabetes in rats in angiotensin II- dependent. *Lab Invest.* 2000;80:513–527.
21. Frustaci A, Kajstura J, Chimenti C, et al. Myocardial cell death in human diabetes. *Circ Res.* 2000;87:1123–1132.
22. Weber KT. Extracellular matrix remodeling in heart failure: a role for de novo angiotensin II generation. *Circulation.* 1997;96:4065–4082.
23. Hayashidani S, Tsutsui H, Ikeuchi M, et al. Targeted deletion of MMP-2 attenuates early LV rupture and late remodeling after experimental myocardial infarction. *Am J Physiol Heart Circ Physiol.* 2003;285:H1229–235.
24. Senzaki H, Paolocci N, Gluzband YA, et al. beta-blockade prevents sustained metalloproteinase activation and diastolic stiffening induced by angiotensin II combined with evolving cardiac dysfunction. *Circ Res.* 2000;86:807–815.
25. Palojoki E, Saraste A, Eriksson A, et al. Cardiomyocyte apoptosis and ventricular remodeling after myocardial infarction in rats. *Am J Physiol Heart Circ Physiol.* 2001;280:H2726–2731.
26. Sam F, Sawyer DB, Chang DL, et al. Progressive left ventricular remodeling and apoptosis late after myocardial infarction in mouse heart. *Am J Physiol Heart Circ Physiol.* 2000;279:H422–428.
27. Oskarsson HJ, Coppey L, Weiss RM, et al. Antioxidants attenuate myocyte apoptosis in the remote non-infarcted myocardium following large myocardial infarction. *Cardiovasc Res.* 2000;45:679–687.
28. Malhotra A, Reich D, Nakouzi A, et al. Experimental diabetes is associated with functional activation of protein kinase C epsilon and phosphorylation of troponin I in the heart, which are prevented by angiotensin II receptor blockade. *Circ Res.* 1997;81:1027–1033.
29. Pfeffer MA, McMurray J, Leizorovicz A, et al. Valsartan in acute myocardial infarction trial (VALIANT): rationale and design. *Am Heart J.* 2000;140:727–750.

Sustained Elevation of Serum Cortisol Level Causes Sensitization of Coronary Vasoconstricting Responses in Pigs In Vivo

A Possible Link Between Stress and Coronary Vasospasm

Takatoshi Hizume, Keiko Morikawa, Aya Takaki, Kohtaro Abe, Kenji Sunagawa, Mutsuki Amano, Kozo Kaibuchi, Chiharu Kubo, Hiroaki Shimokawa

Abstract—Vasospastic angina is induced by stress, for which cortisol secreted by activated hypothalamic/pituitary/adrenal axis may play an important role. However, direct evidence for this notion is still lacking. In this study, we examined whether sustained elevation of serum cortisol level sensitizes coronary vasoconstricting responses in pigs in vivo and, if so, whether Rho-kinase, which we found is a key molecule of coronary vasospasm, is involved. Oral administration of cortisol (20 mg/kg per day) increased its serum level to that seen in restraint stress in pigs. Thus, we examined coronary vasomotor responses in the following 4 groups: (1) control (without cortisol); (2) cortisol (20 mg/kg per day, PO) for 9 days; (3) cortisol plus RU38486 (a glucocorticoids receptor antagonist, 10 mg/kg per day, PO) for 9 days; and (4) cortisol for 9 days followed by 6-week withdrawal. Coronary angiography showed that intracoronary serotonin caused coronary hyperconstriction and reduction in coronary blood flow associated with ischemic ECG changes (coronary vasospasm) in only the cortisol group. All of these responses were abolished by hydroxyfasudil, a specific Rho-kinase inhibitor, in vivo. Organ chamber experiments demonstrated that serotonin concentration-dependently caused hypercontractions of coronary vascular smooth muscle associated with Rho-kinase activation (as evidenced by the enhanced phosphorylation of myosin binding subunit, a substrate of Rho-kinase) in only the cortisol group. All of these responses were again inhibited by hydroxyfasudil in vitro. These results indicate that sustained elevation of serum cortisol level sensitizes coronary vasoconstricting responses through Rho-kinase activation, suggesting the link between stress and coronary vasospasm. (*Circ Res*. 2006;99:767-775.)

Key Words: Rho-kinase ■ coronary vasospasm ■ cortisol ■ myocardial ischemia ■ stress

Physical and/or mental stress induces ischemic attacks in patients with coronary artery disease (CAD). Recent studies have demonstrated that psychological factors are involved in the pathogenesis of CAD[1–4] and that stress could induce coronary vasospasm and myocardial ischemia.[5–7] Indeed, stress test is clinically used to induce vasospastic angina.[8] However, it remains to be examined what component(s) and mechanism(s) of stress are responsible for coronary vasospasm. These points are important to develop an effective therapy to prevent stress-induced myocardial ischemia and sudden death.

Cortisol is among the major stress hormones and is secreted by the activated hypothalamic/pituitary/adrenal axis in physical and/or mental stress.[9–12] Cortisol also could cause endothelial and baroreflex dysfunction.[9,13–15] Short-term oral administration of a high-dose of cortisol impairs endothelial function even in healthy subjects.[14]

Rho-kinase/ROK/ROCK, one of the effectors of the small GTPase Rho, plays an important role in vascular smooth muscle cell (VSMC) contraction.[16–20] In a series of experimental and clinical studies, we have demonstrated that enhanced Rho-kinase activity plays a central role for coronary vasospasm in both animals and humans.[16–20] However, it remains to be examined whether Rho-kinase also is involved in the stress-induced coronary vasospasm.

In the present study, we thus examined whether sustained elevation of serum cortisol level sensitizes coronary vasoconstricting responses in pigs in vivo and, if so, whether Rho-kinase is involved in the molecular mechanism for the sensitization.

Materials and Methods

All procedures were approved by the Institutional Animal Care and Use Committee and were conducted according to the institutional guidelines of Kyushu University.

Original received June 4, 2006; revision received August 11, 2006; accepted August 24, 2006.

From the Departments of Cardiovascular Medicine (T.H., K.M., A.T., K.A., K.S., H.S.) and Psychosomatic Medicine (T.H., C.K.), Kyushu University Graduate School of Medical Sciences, Fukuoka; Department of Cell Pharmacology (M.A., K.K.), Nagoya University Graduate School of Medicine; Department of Cardiovascular Medicine (A.T., H.S.), Tohoku University Graduate School of Medicine, Sendai; and Japan Science and Technology Agency (H.S.), Core Research for Evolutional Science and Technology, Tokyo.

Correspondence to Hiroaki Shimokawa, MD, PhD, Professor and Chairman, Department of Cardiovascular Medicine, Tohoku University Graduate School of Medicine, Seiryo-machi, Aoba-ku, Sendai 980-8574, Japan. E-mail shimo@cardio.med.tohoku.ac.jp

Circulation Research is available at http://circres.ahajournals.org

DOI: 10.1161/01.RES.0000244093.69985.2f

Protocols

A total of 74 male domestic pigs (3 to 5 months, 25 to 30 kg) were used (Kyudo, Tosu, Japan).

Experiment 1: Determination of the Dose of Cortisol

Animals were implanted with a catheter in the jugular vein 5 days before the restraint stress test and were divided into the control, cortisol, and restraint stress groups (n=6 each). The cortisol group was given daily 20 mg/kg of cortisol in drinking water, whereas the other 2 groups were without any medication. The restraint stress group was tethered with a neck chain attached to the small pen (40×100×80 cm) from 8:00 AM to 8:00 PM, and were released from 8:00 PM to 8:00 AM the next morning.[21,22] Blood samples were collected at 3:00 AM, 9:00 AM, 3:00 PM, and 9:00 PM over 24 hours during the experiment. The hourly averages of area under the curve (AUC) of serum cortisol level were evaluated.[23]

Experiment 2: Coronary Vasomotor Responses to Chronic Cortisol Treatment

Pigs were used for coronary angiography (CAG) study (n=26), organ chamber experiments (n=26), and Western blot analysis (n=19). They were housed individually under a controlled room temperature. For CAG study, the animals were divided into the following 4 groups: (1) control group (n=8); (2) cortisol group treated with oral administration of cortisol (20 mg/kg per day) from day 1 to 7 and 9 and 10 (n=8); (3) RU group treated with cortisol (20 mg/kg per day) plus RU38486 (10 mg/kg per day), a glucocorticoid receptor antagonist,[24] on the same schedule as in the cortisol group (n=5); and (4) withdrawal group, which was treated as in the cortisol group, followed by withdrawal of cortisol from day 11 to 55. In the control, cortisol, and RU groups, CAG was performed on day 8, whereas it was performed on both day 8 and 52 in the withdrawal group (n=5). Organ chamber experiment was performed on day 11 in the control, cortisol, and RU groups (n=5 to 8) and on day 55 in the withdrawal group (n=5). All animals were fasted without any medication for 24 hours before the experiments.

Coronary Angiography

Animals were anesthetized with ketamine hydrochloride (15 mg/kg, IM) and pentobarbital (20 mg/kg, IV). They were then intubated and mechanically ventilated with room air. After systemic heparinization (5000 U/body), a preshaped 8F Judkins catheter was inserted through the carotid artery. CAG of the left coronary artery (LCA) was performed in a left oblique view with the cineangiography system (Toshiba Medical, Tokyo, Japan).[19,25,26] ECGs (leads I, II, and III) and arterial pressure were continuously monitored (Nihon Kohden, Tokyo, Japan).[19,25,26] Blood chemistry values (Na, K, Cl, blood urea nitrogen [BUN], creatinine [Cr], glutamate oxaloacetic transaminase [GOT], glutamate pyruvate transaminase [GPT], lactate dehydrogenase [LDH], creatine phosphokinase [CPK]) were also measured. End-diastolic frames were selected to measure coronary diameters. The measurement was made in a blind manner at the left anterior descending coronary artery (LAD), at both the large (just proximal to the first diagonal branch) and small (distal portion of the branch with a baseline diameter of ≈500 μm) coronary arteries.[19,25,26]

Protocols of CAG Study

First, CAG was performed under control conditions. Second, coronary vasomotor responses to serotonin (10 and 100 μg/kg, IC) were examined.[16,19,25,26] Serotonin induces coronary vasospasm that is similar to spontaneous spasm in humans compared with acetylcholine.[27] Third, endothelium-dependent vasodilating responses to bradykinin (0.1 μg/kg, IC) were examined.[25] Fourth, vasoconstricting responses to serotonin (100 μg/kg, IC) were examined after intracoronary infusion of hydroxyfasudil (30 and 100 μg/kg/min for 3 minutes), a specific Rho-kinase inhibitor.[26] Fifth, vasodilating responses to bradykinin (0.1 μg/kg, IC) were examined after intracoronary infusion of N^G-monomethyl-L-arginine (L-NMMA, 1 mg/kg for 10 minutes).[25] Finally, endothelium-independent vasodilating responses to nitroglycerin (10 μg/kg, IC) were examined.[25] CAG was performed 2 minutes after intracoronary administration of serotonin, bradykinin, or nitroglycerin, when the vasodilator or vasoconstrictor effect of each agent peaked.[19,25,26] Each protocol was performed with an interval of 20 to 30 minutes after the confirmation of disappearance of a drug effect by CAG and hemodynamic measurements. Each dose of drugs was diluted with 3 mL of physiological saline, except hydroxyfasudil, which was diluted with 3 mL of distillated water. The degree of coronary vasoconstricting response was expressed as percent change in luminal diameter and blood flow from the baseline values.[19,25,26]

Coronary Blood Flow Measurement

Coronary blood flow velocity was measured by a Doppler guide wire (FloWire, 12 MHz, Cardiometrics, Mountain View, Calif) at the same time with CAG. A 0.014-inch tip Doppler guide wire was advanced via the guiding catheter into the proximal LAD. The position of the Doppler guide wire was kept constant throughout the study. The time average of the spectral peak velocity (APV) was used for mean coronary blood flow velocity.[28] Coronary blood flow was calculated by multiplying a half APV by calculated coronary sectional area at the tip of the Doppler guide wire on the corresponding angiogram.[28]

Organ Chamber Experiments

Three days after the CAG study, animals were sedated with ketamine hydrochloride (15 mg/kg, IM), euphonized with a lethal dose of sodium pentobarbital (40 mg/kg, IV), and then the heart was excised. Epicardial and distal small (≈200 to 250 μm in inner diameter) right coronary arteries (RCA) were carefully dissected and cleaned of any perivascular connective tissue. We used RCA for organ chamber experiments to avoid any influence of CAG on LCA. We have previously confirmed that there are no differences in vascular responses (both in vivo and in vitro) between RCA and LCA,[29] which we also confirmed in the present study (Figure I in the online data supplement, available at http://circres.ahajournals.org). Epicardial RCA were cut into 8 rings (≈4 mm in length),[16,17,25,26] whereas distal small RCA into 8 rings (≈1 mm in length).[30,31] In 4 rings of both-sized arteries, the endothelium was removed by gentle rubbing of the luminal surface with a cotton swab.[17,25,30]

The rings were fixed vertically between hooks in an organ bath containing Krebs–Henseleit solution at 37°C with a mixture of 95% O_2/5% CO_2 and isometric tension was measured with force transducers (Nihon Kohden Inc). KCl solution (62 mmol/L) was applied every 15 minutes until the amplitude of contraction reached a constant value. The developed tension was expressed as a percentage of that attained in the last precontraction with 62 mmol/L KCl.[17,25,30] The presence and absence of the endothelium was confirmed by the presence and absence of relaxation to bradykinin (10^{-7} mol/L) during a contraction evoked by KCl, respectively.[25]

The direct VSMC vasocontracting effect of serotonin (10^{-9} to 10^{-5} mol/L) was evaluated in rings without endothelium.[17,26] The acute inhibitory effect of hydroxyfasudil on serotonin-induced VSMC contraction was examined after equilibration with hydroxyfasudil (10^{-6} and 3×10^{-6} mol/L, for 30 minutes) separately in different rings without endothelium.[17,26] Endothelium-dependent relaxations to bradykinin (10^{-11} to 10^{-6} mol/L) were examined in rings with endothelium during a contraction evoked by prostaglandin (PG) $F_{2\alpha}$ (2×10^{-6} mol/L). The extent of contraction in response to $PGF_{2\alpha}$ was adjusted to 50% to 70% of that induced by 62 mmol/L KCl.[25,30,31] The contribution of vasodilator PGs, nitric oxide (NO), and endothelium-derived hyperpolarizing factor (EDHF) to endothelium-dependent relaxations to bradykinin was evaluated by determining the inhibitory effect of indomethacin (10^{-5} mol/L), N^{ω}-nitro-L-arginine (L-NNA, 10^{-4} mol/L), and charybdotoxin (an inhibitor of large and intermediate-conductance KCa channels, 100 nmol/L) plus apamin (an inhibitor of small conductance KCa channels, 1 μmol/L), respectively.[30,31] Endothelium-independent relaxations to sodium nitroprusside (SNP) (10^{-10} to 10^{-5} mol/L) also were examined in rings without endothelium.

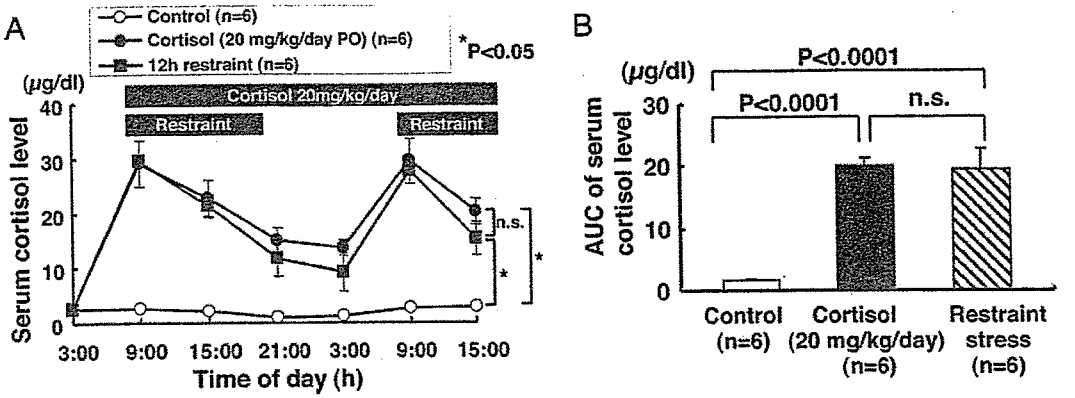

Figure 1. Daily profile (A) and areas under the curve (AUC) (B) of serum cortisol level during restraint stress and oral administration of the hormone. The oral administration of cortisol significantly increased serum cortisol level, equivalent to that in restraint stress. Results are expressed as mean±SEM. n.s. indicates not significant.

To evaluate the acute effect of cortisol on coronary vasomotor responses, organ chamber experiments were also performed in rings with or without endothelium from normal coronary arteries in the absence and presence of cortisol (10 and 30 μg/dL for 60 minutes and 30 μg/dL for 120 minutes).

Histopathology

LCA were perfused via constant-pressure perfusion system (120 cm H_2O) with saline (1000 mL) and subsequently with 5% formaldehyde (1000 mL).[19,32] After fixation, LAD was cut transversely, dehydrated, embedded in paraffin, and cut into 5-μm-thick slices. These segments were stained with hematoxylin/eosin and van Gieson's elastic staining for histological analysis.

Western Blot Analysis for Rho-Kinase Activity

Rho-kinase activity can be evaluated by the extent of phosphorylation of myosin-binding subunit (MBS) of myosin phosphatase, a substrate of Rho-kinase.[16,32–34] The regions containing MBS were visualized by ECL Western blotting luminal reagent (Santa Cruz Biotechnology, Santa Cruz, Calif).[16,17,32] Isolated RCA rings without endothelium were subjected to SDS-PAGE immunoblot analysis when serotonin-induced (10^{-6} mol/L) contraction reached a maximum.[16,17,32] Rho-kinase activity is expressed by the extent of MBS phosphorylation when normalized to total MBS.

Statistical Analysis

Results are expressed as mean±SEM. χ^2 test was used for comparison of ECG ST-segment changes. Results of CAG and blood flow were analyzed by 2-way ANOVA followed by Bonferroni test for multiple comparisons. Serum cortisol levels under control condition and during oral administration of cortisol and restraint stress, AUC of serum cortisol level, and the results of organ chamber experiments were analyzed by 2-way ANOVA, followed by Scheffe test for multiple comparisons. The results of Western blot analysis were analyzed by Dunnet test. A value of $P<0.05$ was considered to be statistically significant.

Results

Daily Profile of Serum Cortisol Level During Restraint Stress and Oral Administration

Daily profile (Figure 1A) and AUC (Figure 1B) of serum cortisol levels were comparable between restraint stress and oral administration of the hormone.

Coronary Vascular Responses to Serotonin In Vivo

Among the control, cortisol, and RU groups, hemodynamic variables (heart rate and blood pressure) (supplemental Table I) and blood chemistry values (data not shown) were comparable. Because cortisol was stopped 24 hours before the CAG experiment, the serum cortisol level (μg/dL) was comparable among the 3 groups (2.4±0.8 in the control, 1.9±0.5 in the cortisol, and 2.1±0.7 in the RU group, n=5 each).

There was no significant difference in baseline coronary diameter among the 3 groups (supplemental Table II). A low dose of serotonin (10 μg/kg, IC) caused mild coronary vasodilatation without any significant ECG changes in the control (Figure 2A through 2D) and RU (Figure 2I through 2L) groups but caused intense and diffuse vasoconstriction, especially at small coronary arteries, with ischemic ST changes in the cortisol group (ST elevation in 3/5 and ST depression in 1/5) (Figure 2E through 2H). By contrast, a high dose of serotonin (100 μg/kg, IC) caused coronary vasoconstriction in large (Figure 3G) and small (Figure 3H) arteries in all the 3 groups; however, the extent of the vasoconstriction was most prominent in the cortisol group, especially at small coronary arteries (Figure 3G and 3H). Intracoronary pretreatment with hydroxyfasudil dose-dependently suppressed the serotonin-induced vasoconstrictions in all the 3 groups (Figure 3).

Coronary blood flow was slightly increased in response to a low dose of serotonin but was decreased to a high dose of serotonin in the control and RU groups (Figure 3I). By contrast, in the cortisol group, coronary blood flow was decreased in response to both doses of serotonin, which was again dose-dependently inhibited and was converted to an increase in the flow by hydroxyfasudil, as seen in other 2 groups (Figure 3I).

Coronary Endothelial Vasodilator Function In Vivo

Bradykinin (0.1 μg/kg, IC) caused mild coronary vasodilatation in both-sized arteries and an increase in coronary blood flow in all the 3 groups (Figure 4). Pretreatment with intracoronary L-NMMA tended to inhibit the bradykinin-induced coronary vasodilatation in all groups, whereas nitroglycerin (10 μg/kg, IC) caused a comparable extent of coronary vasodilatation and increase in coronary blood flow in all groups (Figure 4).

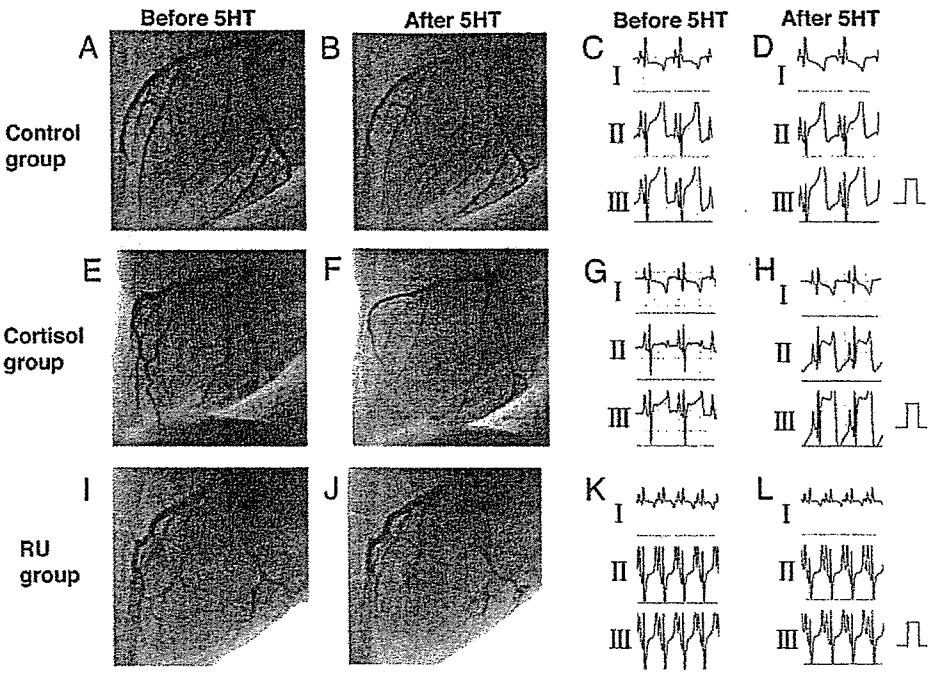

Figure 2. Coronary angiograms and ECG before and after a low dose of serotonin (5HT) (10 μg/kg, IC). Serotonin induced mild coronary vasodilatation with no ischemic ECG changes in the control (A through D) and RU (I through L) groups but induced diffuse and intense coronary vasoconstriction with ischemic ST changes in the cortisol group (E through H). Calibration on ECG, 1 mV.

Effect of Withdrawal of Long-Term Treatment With Cortisol

In the withdrawal group, there was no significant difference in basal coronary diameters as compared with other 3 groups (supplemental Table I) or between day 8 (before cessation of the cortisol treatment) and day 52 (6 weeks after withdrawal) (supplemental Table III). On day 8, intracoronary serotonin again caused intense and diffuse coronary vasoconstriction (Figure 5A and 5B), whereas on day 52, the hyperconstrictions were no longer noted (Figure 5C and 5D). On day 8 and 52, hydroxyfasudil again inhibited the serotonin-induced coronary vasoconstriction and the decrease in coronary blood flow (Figure 5E through 5G).

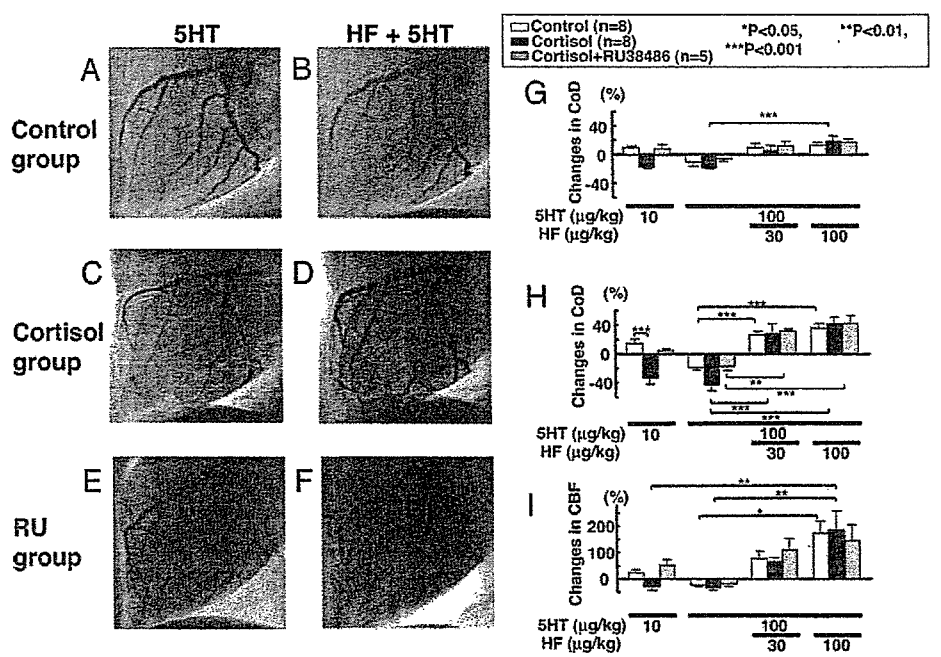

Figure 3. Inhibitory effects of hydroxyfasudil on serotonin-induced coronary vasospasm. Serotonin (5HT) (10 and 100 μg/kg, IC) caused hyperconstriction in both large (G) and small (H) coronary arteries in the cortisol (C) but not in the control (A) or RU (E) group. Hydroxyfasudil (HF) (100 μg/kg, IC) abolished the serotonin-induced vasoconstriction and converted the vasoconstriction to vasodilatation in all groups (B, D, F, G, and H). Similarly, HF converted the serotonin-induced reduction in coronary flow to an increase in the flow in the cortisol group (I). CoD indicates coronary diameter; CBF, coronary blood flow. Results are expressed as mean±SEM.

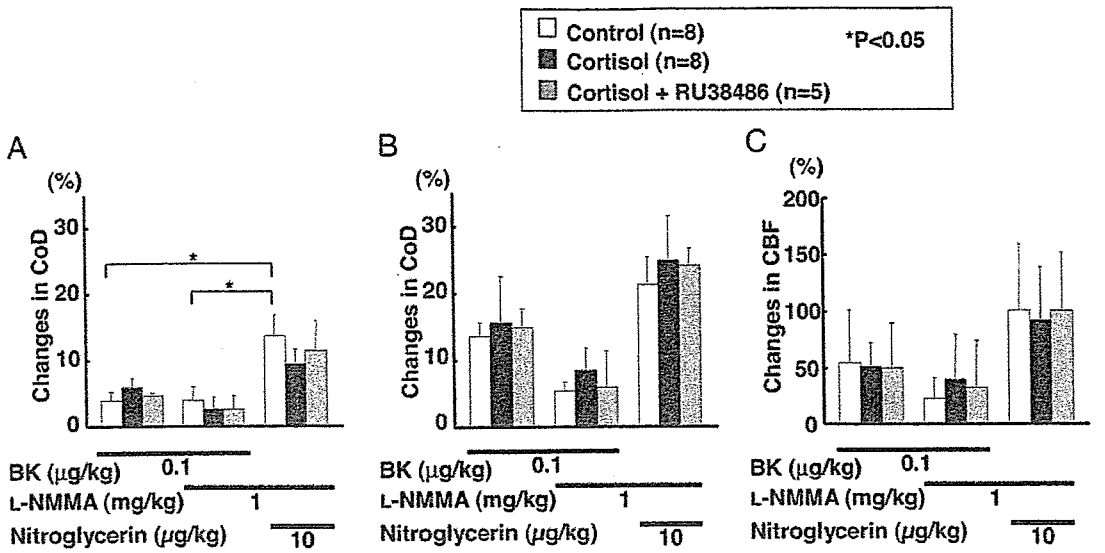

Figure 4. Assessment of coronary endothelial vasodilator functions in vivo. Bradykinin (BK) (0.1 μg/kg, IC) caused a comparable extent of coronary vasodilatation in both large (A) and small (B) coronary arteries and coronary flow (C) among the 3 groups. L-NMMA did not significantly inhibit the bradykinin-induced coronary vasodilatation in all groups. Intracoronary nitroglycerin (10 μg/kg) also caused a comparable extent of coronary vasodilatation among the 3 groups. CoD indicates coronary diameter; CBF, coronary blood flow. Results are expressed as mean±SEM.

Organ Chamber Experiments

Serotonin caused concentration-dependent contractions of coronary rings without endothelium from both-sized arteries (Figure 6). The extent of the contractions was significantly greater in the cortisol group compared with other 3 groups in both-sized coronary arteries (Figure 6A and 6D). Hydroxyfasudil significantly suppressed the serotonin-induced hypercontractions of both-sized arteries (Figure 6B and 6E). No

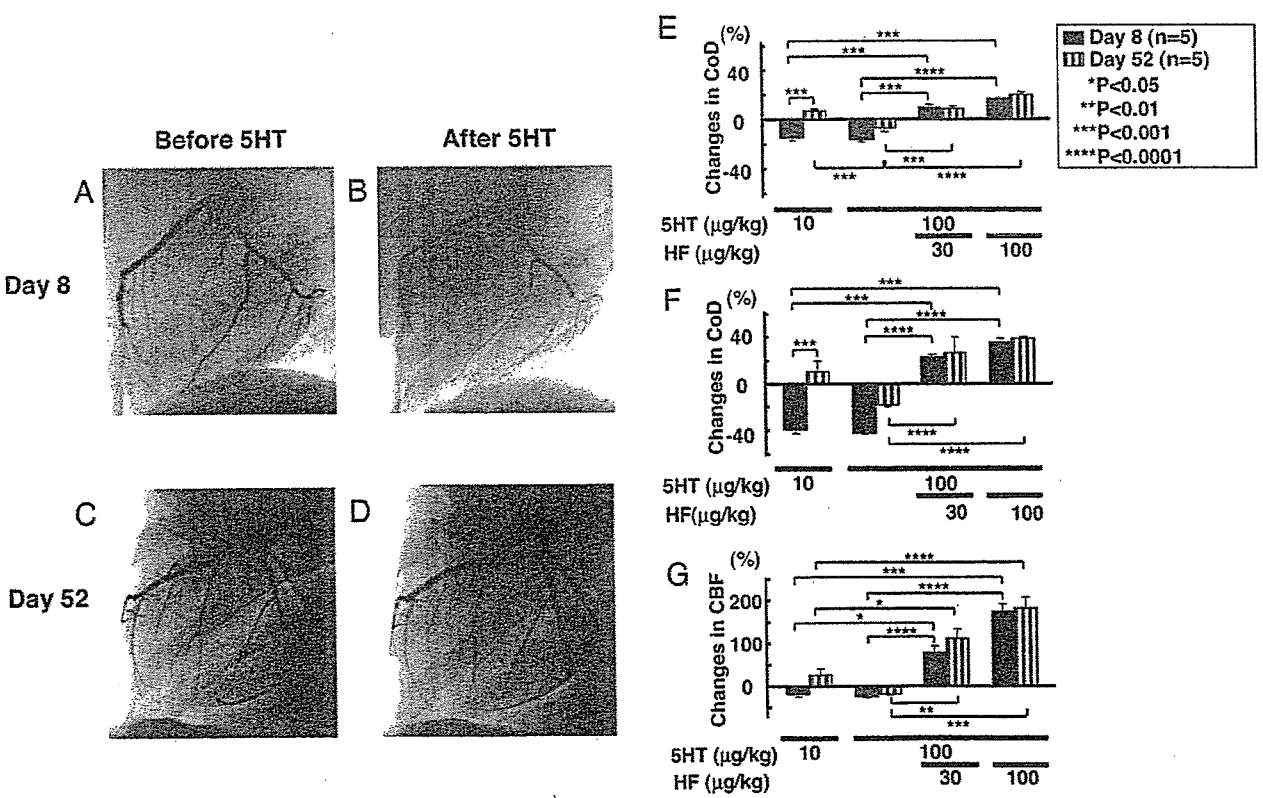

Figure 5. Effects of cessation of chronic cortisol treatment. After confirmation of the serotonin (5HT)-induced coronary vasospasm on day 8 (A and B), the cortisol treatment was stopped. On day 52, the serotonin-induced vasospasm was no longer noted (C and D). Comparisons between day 8 and 52 are shown for coronary vasoconstriction in large (E) and small (F) coronary arteries and coronary flow (G). CoD indicates coronary diameter; CBF, coronary blood flow; HF, hydroxyfasudil. Results are expressed as mean±SEM.

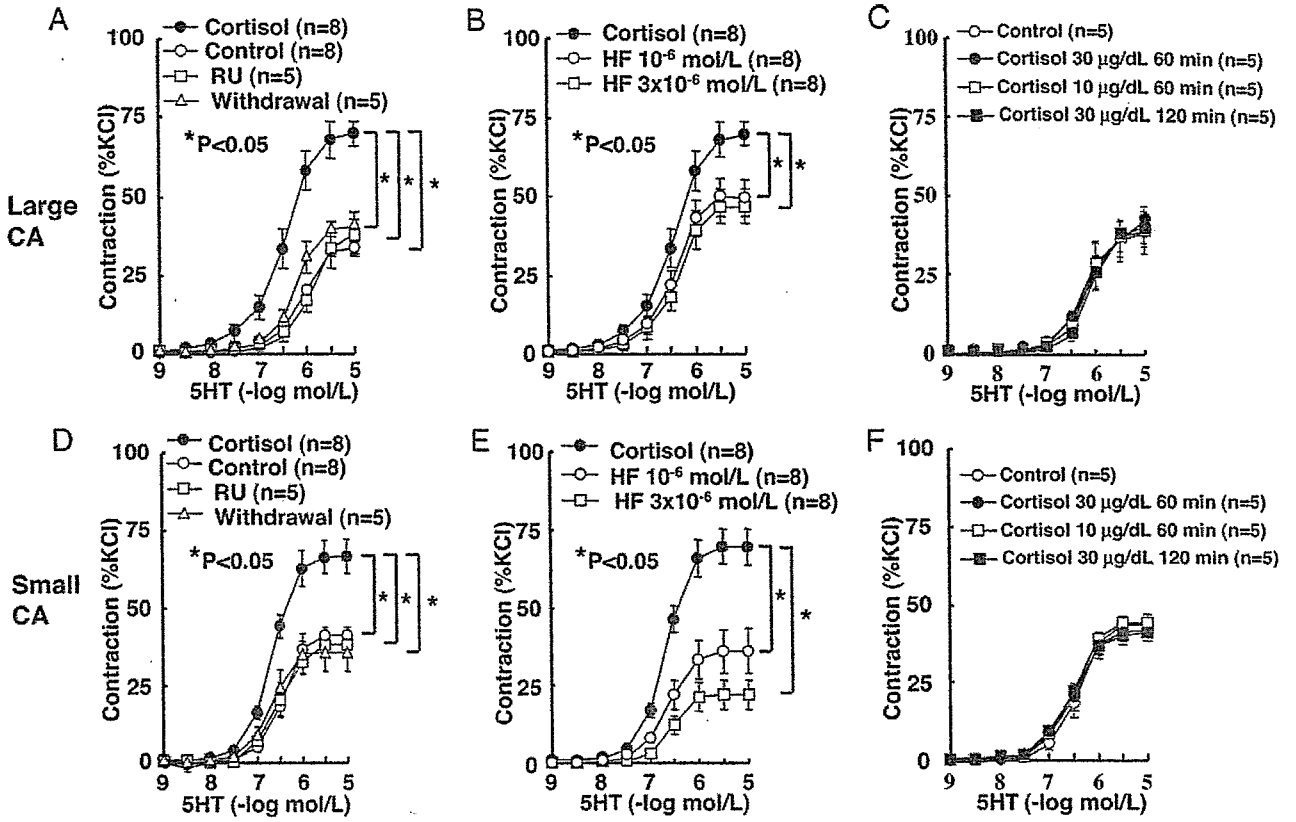

Figure 6. Acute and chronic effects of cortisol on serotonin-induced coronary VSMC contractions in vitro. The chronic cortisol treatment enhanced serotonin-induced VSMC contractions in both large (A) and small (D) coronary arteries (CA) compared with other 3 groups, which were significantly inhibited by hydroxyfasudil (HF) in both large (B) and small (E) coronary arteries. By contrast, no acute effects of the hormone were noted in large (C) or small (F) coronary arteries. Results are expressed as mean±SEM.

acute effects of cortisol on serotonin-induced contractions of normal coronary rings were noted (Figure 6C and 6F).

Endothelium-dependent relaxations to bradykinin were comparable among the 4 groups in both-sized arteries under the 4 different conditions (supplemental Table IV), and no acute effects of cortisol on endothelium-dependent relaxations of normal coronary rings were noted (supplemental Table V). Endothelium-independent relaxations to SNP also were comparable among the 4 groups in both-sized coronary arteries (supplemental Table VI).

Histopathology

There were no obvious histological changes (eg, intimal thickening or inflammatory cell infiltration) in any of the 4 groups (n=5 each, data not shown).

Western Blot Analysis

The extent of MBS phosphorylation, a marker of Rho-kinase activity, was enhanced in response to serotonin only in the cortisol group, and was dose-dependently inhibited by hydroxyfasudil (Figure 7). By contrast, in other 3 groups, the serotonin-induced Rho-kinase activation was absent and no inhibitory effects of hydroxyfasudil were noted (Figure 7). There was a significant positive correlation between the extent of MBS phosphorylation (Rho-kinase activity) and that of the serotonin-induced contractions among the 4 groups studied (Figure 8A) and the inhibitory effects of hydroxyfasudil on the serotonin-induced activation of Rho-kinase was confirmed (Figure 8B).

Discussion

The novel findings of the present study are that sustained elevation of serum cortisol level causes sensitization of coronary VSMC constricting responses to serotonin both in vivo and in vitro and that Rho-kinase–mediated pathway is substantially involved in the molecular mechanisms for the sensitization. To the best of our knowledge, this is the first study that demonstrates the link between elevated serum cortisol level and hyperconstriction of coronary VSMCs through Rho-kinase activation in vivo.

Sustained Elevation of Serum Cortisol Level and Rho-Kinase Activity

We have demonstrated that Rho-kinase is upregulated in spastic coronary segment, which leads to inhibition of myosin light chain (MLC) phosphatase with resultant enhancement of MLC phosphorylation and VSMC contraction.[16,18,26,35] In the present study, we were able to demonstrate that sustained elevation of serum cortisol level enhances coronary vasospastic activity through Rho-kinase activation. Serotonin exerts 5-HT_{2A} serotonergic receptor– and Rho-kinase–mediated direct vasoconstrictor effects and 5-HT_{1B} serotonergic receptor–mediated endothelium-dependent relaxations in porcine coronary arteries.[36] In the present study, a specific Rho-kinase

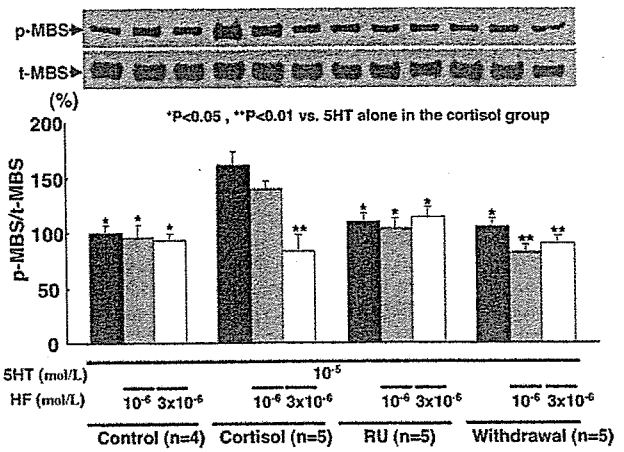

Figure 7. Cortisol-induced Rho-kinase activation in coronary VSMCs. Rho-kinase activity, as evaluated by phosphorylated MBS/total MBS ratio, was significantly enhanced in the cortisol group during serotonin-induced contraction compared with other 3 groups, which was concentration-dependently inhibited by hydroxyfasudil (HF). Results are expressed as mean±SEM.

inhibitor, hydroxyfasudil, unmasked endothelium-dependent vasodilatation and increase in coronary blood flow in response to serotonin through inhibition of the Rho-kinase–mediated direct vasoconstrictor effects of the monoamine.

In this study, the cortisol treatment was stopped 24 hours before the experiment to avoid any acute effects of the hormone. Moreover, cortisol had no acute effect on coronary vasoconstricting responses in vitro. Thus, the sensitization of coronary vasoconstricting responses is apparently attributable to chronic effects of cortisol on Rho-kinase activity in coronary VSMCs.[16,18,26,35] The finding that withdrawal of cortisol resulted in the disappearance of coronary hyperconstricting responses both in vivo and in vitro associated with normalization of coronary Rho-kinase activity further supports this notion.

In the present study, endothelial vasodilator function per se was preserved, whereas VSMC contraction was enhanced in response to the chronic elevation of serum cortisol level in both-sized coronary arteries. However, the decrease in coronary flow secondary to enhanced vasoconstriction in coronary resistance vessels could, at the same time, amplify the net vasoconstriction by reducing shear stress induced vascular relaxation. The mechanism for the enhanced coronary vasoconstricting responses caused by sustained elevation of serum cortisol level is apparently attributable to VSMC hyperreactivity that exceeds endothelial vasodilator capacity, a consistent finding with our previous studies.[25,35,36] In the present study, coronary endothelial vasodilator function in response to bradykinin was relatively resistant to the blockade of NO synthesis in both-sized arteries both in vivo and in vitro. This finding also is consistent with our previous findings that endothelium-dependent relaxation to bradykinin is largely mediated by EDHF.[20,37] However, it remains to be examined whether EDHF-mediated responses also are impaired in response to a long-term increase in serum cortisol levels.

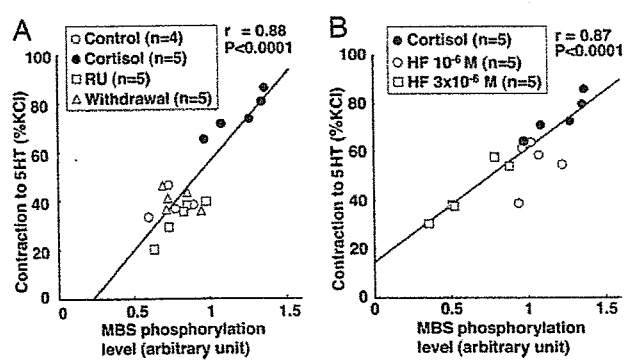

Figure 8. Correlation between the extent of MBS phosphorylation and that of serotonin-induced contractions in the control, cortisol, RU, and withdrawal groups (A) and in the absence (cortisol) and presence of hydroxyfasudil (HF) (B). There were significant positive correlations between the 2 values.

Cortisol and CAD

There is a line of evidence for the link between cortisol and CAD. The 5-year incidence of cardiovascular events was significantly higher in men with abnormal cortisol secretion compared with those with a normal pattern.[38] In addition, increased serum cortisol level in patients with depression enhances prothrombotic state[2] and increases the density of 5-HT_2 serotonergic receptors in platelets, a useful index of platelet activation.[39] Cortisol also could accelerate atherosclerotic process[40]; however, no atherosclerotic changes were noted in the present study, probably because of the relatively short treatment period.

Role of Cortisol in the Pathogenesis of Stress-Induced CAD

Environmental and/or psychological factors contribute to the pathogenesis of CAD.[1–4] It is known that serum levels of cortisol are frequently and chronically elevated in humans with stress and are also normalized after stress is resolved.[41–44] Indeed, natural and/or social disasters have been associated with a transient increase in ischemic cardiac events after the disasters.[45–48]

Coronary vasospasm could be induced in either a focal form or a diffuse form.[36] The latter form may be more frequently associated with myocardial ischemia because of more increased coronary vascular resistance.[36] In the present study, the sustained increase in serum cortisol level sensitized coronary VSMC constricting responses and caused a diffuse form of coronary vasospasm with myocardial ischemia, suggesting an increased risk of myocardial ischemia and sudden death in stress.

Cortisol is secreted by the activated hypothalamic/pituitary/adrenal axis and plays a key role in stress.[11,12] Elevated plasma and urinary levels of corticosteroids and a disturbed diurnal cortisol rhythm have been documented in a variety of diseases with mental stress, including depression, which is among the important risk factors of cardiovascular disease.[10–12] Stress may be closely related to vasospastic angina[6,8]; however, no direct evidence has yet been provided for the link between stress and coronary vasospasm. The present study suggests that Rho-kinase–mediated sensitization of coronary VSMC constricting responses caused by elevated